Response of a Stably Stratified Oceanic Bottom Boundary Layer on a Slope to Time Dependent Forcing

by

David Ramsden

B. Eng. McMaster University, 1972

A THESIS SUBMITTED IN PARTIAL FULFILLMENT OF
THE REQUIREMENTS FOR THE DEGREE OF
MASTER OF SCIENCE
in the School of Earth and Ocean Sciences

We accept this thesis as conforming to the required standard

[redacted]

Dr. C. J. R. Garrett, Supervisor (SEOS)

[redacted]

Dr. D. Lobb, Outside Member (Physics)

[redacted]

Dr. A. Weaver, Additional Member (SEOS)

[redacted]

Dr. W. Crawford, Additional Member (IOS)

[redacted]

Dr. L. Maas, Outside Examiner (SEOS)

Supervisor: Dr. C. J. R. Garrett

ABSTRACT

The behaviour of time-dependent oceanic boundary layers on a sloping bottom in the presence of stratification is investigated by the method of direct numerical simulations. The Navier-Stokes equations are decomposed into mean and turbulent components with the mean equations expressed in terms of a slope Burger number: $S = N^2 \sin^2\theta / f^2$, where N is the buoyancy frequency, θ is the bottom slope angle, and f is the Coriolis parameter. The influence of the turbulent fluctuations is parameterized as eddy coefficients of viscosity and diffusivity.

Three regimes are considered. The first is for cases where the eddy coefficients are constant in time but variable in space and the interior flow is allowed to adjust to the boundary mixing. The numerical results agree with analytic theory for two limiting cases. The first case is when the mixing extends into the fluid interior and the second is when the mixing is limited to a slab region.

The second regime involves cases in which the eddy coefficients are determined from a gradient Richardson number hypothesis. The interior alongslope flow is fixed in time. Two cases are considered and it is shown that the resultant Ekman layer shutdown from downwelling favourable flows can be parameterized in terms of the Burger number and a 'stratification drag' number $D = C_d N/f$, where C_d is the bottom drag coefficient.

Cases which are favourable to downwelling flow are shown to shut down in a time proportional to $S^{-\frac{3}{2}} D^{-1} f^{-1}$. Cases which are favourable to upwelling flow are also investigated. The results are shown to depend on the values of diffusivity in the well-mixed and far-field region. The results, though not conclusive, suggest upwelling favourable flows shut down in a time initially proportional to $S^{-1} D^{-\frac{1}{2}} f^{-1}$.

The third regime considers cases in which the interior alongslope flow is time dependent and all other variables adjust to the forcing. For several cases of the boundary conditions and flow parameters, the mixed layer is shown to mix and restratify in the course of a forcing cycle, with mixing due to average buoyancy fluxes no greater than primary mixing rates.

[redacted]

Dr. C.J.R. Garrett, Supervisor (SEOS)

[redacted]

Dr. D. Lobb, Outside Member (Physics)

[redacted]

Dr. A. Weaver, Additional Member (SEOS)

[redacted]

Dr. W. Crawford, Additional Member (IOS)

[redacted]

Dr. L. Maas, Outside Examiner (SEOS)

Acknowledgements

I thank Hide Yamazaki for the use of an X terminal and for supplying much of the computational resources necessary to complete this project. I thank Patrick Cummins for help with the Crank-Nicholson timestepping, for supplying extra CPU cycles on his HP730 workstation and for other tangible and intangible support. I thank Chris Garrett for the opportunity to return to graduate school and for maintaining his good will when it looked like I might not be able to complete the project.

Finally, I thank my wife and children for their support and encouragement during the down times (When are you going to get a *real* job, dad?), and particularly to my wife, Joyce, for just being herself.

Examiners

.....
Dr. C.J.R. Garrett, Supervisor (SEOS)

.....
Dr. D. Lobb, Outside Member (Physics)

.....
Dr. A. Weaver, Additional Member (SEOS)

.....
Dr. W. Crawford, Additional Member (IOS)

.....
Dr. L. Maas, Outside Examiner (SEOS)

Contents

List of Tables

List of Figures

List of Symbols

Symbol	Description	Symbol	Description
X	Alongslope direction	x	Nondimensional X
Y	UpSlope Direction	y	Nondim. Y
Z	Dir. Normal to Slope	z	Nondim. Z
T, t	Dim. and Nondim. Time	g	gravity
H, h	Scale Height	f	Coriolis Parameter
$\overline{P}$	Pressure	p	Nondimensional Pressure
U, u	Alongslope Velocity	V, v	Upslope Velocity
ρ_0	Reference Density	$\overline{\rho}$	Mean Density
B	Mean Buoyancy	b	Nondim. Mean Buoyancy
N	Buoyancy Frequency	b'	Pertubation Buoyancy
θ	Bottom Slope	C_d	Bottom drag Coefficient
S	$\frac{N^2 \sin^2 \theta}{f^2}$	Ri	Richardson Number
ν	Dim. Eddy Viscosity	ν'	Nondim. Eddy Viscosity
κ	Dim. Eddy Diffusivity	κ'	Nondim. Eddy Diffusivity
Pr	ν/κ	E	Ekman Number
u_∞	Velocity Jump	u_e	u in the Far Field
$q^{-1} = h_t$	Thorpe Scale	h_p	Pollard *et al* Scale
ϵ	Ratio of near and far-field ν	δ	ν Shaping Parameter
D	$\frac{C_d N}{f}$	β	$D/\sqrt{2}$
Tr	Integrated Ekman Flux	Tr_0	Initial Ekman Flux
ω	Forcing frequency in units of f	$M2$	Tidal Frequency

Table 0.1: List of Symbols

Chapter 1

Introduction

1.1 Where Does Mixing Occur in the Ocean?

There is a popular saying to the effect that the history of science has been the history of measurement. This is probably somewhat unfair as many observations have been successfully predicted and directed by theoretical considerations. When considering new phenomena, however, the popular saying has some validity. Traditionally, scientists have ascribed uniformity and simplicity to terrestrial regimes until direct or indirect evidence causes them to seek better analogies and more complex models and often those original models are shown to be completely wrong.

This has certainly been true of the ocean. It was not so long ago that the abyssal ocean was viewed by many as a uniform and quiescent medium. With the advent of deep-sea hydrographic and current measurement techniques, it has been subsequently discovered (e.g. Mantyla and Reed [1]) that deep boundary currents exist and that turbulent, well mixed-layers exist above bottom slopes, which vary greatly in their height over the course of time (e.g. Armi and Millard [3] and Thorpe *et al*, [4]).

The deep ocean possesses a spatially and temporally fairly uniform vertical temperature and salinity structure. With information about deep water formation and the temperature structure, Munk [5] derived an eddy diffusivity of heat necessary

to balance the slow upwelling of cold Antarctic bottom water. This value, about $10^{-4}m^2/s$, presented both a conclusion and a challenge to oceanographers. Munk's model assumed spatial and temporal uniformity of the slow upwelling of the Antarctic bottom water over the whole ocean and could only be considered applicable where other effects may not be important.

Where available, more direct measurements of eddy coefficients of diffusivity based on microstructure data in the open ocean (e.g. Gregg [6]) seem to indicate values closer to $10^{-5}m^2/s$, at least in the upper 1000 metres of the ocean. The situation is complicated somewhat by the knowledge that turbulent mixing events (with higher values of diffusivity) in the upper thermocline are highly sporadic (Yamazaki and Lueck [7]). It is unlikely, though, that the time and space averages over these events will change the 10^{-5} value significantly, as they lack spatial and temporal extent except in equatorial regions where mixing is stronger.

Munk's model is based on a balance between advection (vertical velocities) and diffusion, and is probably not true in the upper thermocline as ventilation is the more likely mechanism. The rationale for this assumption is that surface heat fluxes will warm the surface layers which will be then be transported along isopycnal surfaces into the ocean interior. No diapycnal mixing need occur and eddy diffusivities do not need to be of order $10^{-4}m^2/s$.

In the deeper ocean, direct measurements of advective/diffusive balances in ocean basins do seem to indicate values of $10^{-4}m^2/s$, (Hogg *et al*, [8]). There is not any clear idea of how to resolve the differences in the balance calculations and the directly measured values except to speculate some depth dependence on diffusivity (e.g. Gargett, [9]), or 'other' mechanisms.

In the deeper ocean, are the balances achieved by advection/diffusion, or is the fluid being mixed in isolated places and then laterally stirred? Some localized mixing mechanisms proposed have included double diffusion, turbulence at the edge of interleaving water masses, critical reflection and breaking of internal waves, and boundary mixing. Garrett [10] gives a review of these possible mechanisms, elimi-

nating many of them, and concludes that near boundary mixing may be the only possible viable candidate, at least in the deeper parts of the ocean. This would imply that mixing rates near oceanic boundaries would have to sufficiently strong that when laterally stirred into the ocean's interior, it would provide enough heat flux for entire ocean basins.

The determination of the vertical eddy diffusivity is of more than pure academic interest. With the development of large numerical models to simulate the motion of the world's oceans as a necessary component of overall climate models, a value (or a formula for spatially and temporally variable values) of the vertical eddy diffusivity, is needed. Bryan [11] has found great sensitivity of primitive equation models to the values of vertical eddy diffusivity, though the values used are chosen for numerical stability reasons. Cummins *et al* [12] also show that problems with proper representation of the thermocline, and poleward heat flux in the same models, are related to small changes in the values of vertical eddy diffusivity, though they investigated a depth dependence.

Also, with the current interest in greenhouse gases, the uptake of these gases by the ocean could be a key factor in moderating 'CO_2 doubling' scenarios and their effect on world climate, if it is assumed the eddy diffusivities of heat and gases are the same. Finally, if there is residual flow from boundary mixing, it may have consequences for the spreading of wastes which have been dumped on continental slopes.

1.2 Boundary Mixing?

Citing evidence for detached mixed layers from a boundary, and following a suggestion first put forward by Munk [5], Armi [13] postulated that perhaps boundary mixing could provide the necessary heat flux to balance the global ocean heat equation. In this theory, the mixed boundary water is advected (moved by the local flow field) into the ocean's interior along isopycnal (constant density) surfaces. The effective eddy diffusivity is calculated by scaling the eddy diffusivity of the boundary

mixing by the relative areas of the boundary and world oceans. By this assumption, no vertical heat transfer need occur in the ocean's interior.

There are problems with this theory, however. Garrett [10] pointed out that boundary mixing may not be very effective, since mixing well-mixed water does not generate the vertical buoyancy fluxes necessary for net mixing. Phillips *et al* [14] demonstrated, that in a laboratory, restratification occurred near the boundary, which could result in upslope transports. Whether this result is applicable to the ocean is debatable because of the strong effect of the boundary in laboratory experiments. Garrett [16] also points out that the restratification may not generate the necessary *vertical* buoyancy fluxes. This assertion was followed by the subsequent calculation (Garrett, [17]) of the amount of net mixing from boundary layers which fully mix and then restratify. Garrett [17] found that the net mixing would probably be small, even when net upslope or downslope movement during the mixing cycle was considered.

At issue is the physics of boundary layers on a slope. Much of the theoretical work on the subject has assumed stationarity and that the eddy coefficients of viscosity and diffusivity are constant in time, permitting solutions to the equations of motion (e.g. Thorpe [15], Garrett [17]). These equations predict values of the along and alongslope flow induced by the mixing for idealized parameters, and it would be desirable to test them in some way and estimate their range of usefulness.

There is another aspect of oceanic bottom boundary layers which provides another example of measurements inspiring theory. It has been found that the Greenland Current penetrates much farther down the eastern coast of North America than would be predicted from standard Ekman theory (e.g. MacCready and Rhines [2], hereafter MR92). MR92 and Trowbridge and Lentz, [18], hereafter TL, investigated various aspects of Ekman layer 'shutdown' which would occur as buoyancy forces shut down the Ekman transport. As part of their models, the mixed layers evolve in time in response to a constant alongslope flow, and both studies showed asymmetries in the responses to upwelling and downwelling favourable forcing.

These studies indicated that buoyancy forces could indeed replace drag forces and allow a boundary current to propagate as if no drag existed at all. This happens as a result of initial Ekman transports carrying heavy water up the slope, or pushing light water down the slope which results in a buoyancy force opposing further Ekman flux. In the process, the near boundary alongslope flow goes to zero by a thermal wind balance which is an adjunct to the Ekman layer shutdown.

These studies suffer from deficiencies, however, in terms of the proper representation of the evolution of the mixed layer, or the amount of drag induced at the boundary. A more complete description of Ekman layer shutdown for the case of constant interior alongslope flow would be desirable. In particular, this thesis would like to determine the dimensionless parameters which govern the Ekman layer shutdown processes.

Finally, as mentioned before, there is much temporal variability in the thickness of the mixed layer. Another intent of this thesis is to make progress towards a consistent theory of bottom boundary layers which can thicken and thin in response to variable interior alongslope flow or other interior flow parameters. At issue is the physics of restratification (which will be partially dealt with in treatment of the upwelling favourable flow). Ideally, an estimation of net vertical buoyancy fluxes from (e.g.) tidal cycles as functions of relevant dimensionless parameters, is desired. If possible, a comparison of numerical and theoretical results to measurements is also desired.

1.3 Objectives of the Thesis

The aims of this thesis are to investigate various aspects of oceanic bottom boundary layers on a sloping bottom in the presence of stable stratification. More specifically,

1. Develop a numerical model which can test the predictions of some of the analytic theories. For example:

- Do the model and theories agree when 'ideal' theoretical parameters are used?

- As the parameters are relaxed away from ideal values, what is the degree to which the analytic predictions are in error?

- How long does it take the numerical simulations to approach the theoretical values?

2. Modify the methods of MR92 and TL for more realistic physics and develop a consistent theory of Ekman layer shutdown.

   - Determine the dimensionless parameters and timescales that govern the Ekman layer shutdown process for downwelling favourable flows.

   - For upwelling favourable flows, attempt to describe aspects of the shutdown process and the anticipated thinning of the mixed layer.

3. Develop a model which can respond to variable alongslope flow and investigate the physics of the response of the bottom layer to the forcing cycle for:

   - Purely tidal forcing (no mean component) driven by an alongslope velocity.

   - Alongslope flow driven by a pressure gradient.

4. In both cases, determine net mixing and upslope movement over a forcing cycle in a limited parameter space.

Chapter 2

The Model Equations

Figure 2.1, adapted from Garrett, MacCready and Rhines [19], hereafter GMR, shows a definition sketch of the bottom boundary region. On basis vectors X, Y and Z, with Z directed normal to the bottom slope at an angle θ, and Y parallel to the bottom slope gradient. $V = V(Z,T)$ is upslope velocity and $U = U(Z,T)$ is alongslope (out of the page).

The Navier-Stokes equations are decomposed into mean and fluctuating parts. If it is assumed that the timescales of the mean parts are sufficiently longer than that of the fluctuating parts (a sufficient spectral gap), then the mean equations of motion can be written as

$$\frac{\partial U}{\partial T} - fV = -\frac{1}{\rho_0}\frac{\partial \overline{P}}{\partial X} + \frac{\partial}{\partial Z}\left(\nu \frac{\partial U}{\partial Z}\right) \tag{2.1}$$

$$\frac{\partial V}{\partial T} + fU = -\frac{1}{\rho_0}\frac{\partial \overline{P}}{\partial Y} + B\sin\theta + \frac{\partial}{\partial Z}\left(\nu \frac{\partial V}{\partial Z}\right) \tag{2.2}$$

$$0 = -\frac{1}{\rho_0}\frac{\partial \overline{P}}{\partial Z} + B\cos\theta - \frac{\partial}{\partial Z}(\overline{W^2}) \tag{2.3}$$

$$\frac{\partial B}{\partial T} + VN^2\sin\theta = \frac{\partial}{\partial Z}\left(\kappa \frac{\partial B}{\partial Z}\right) \tag{2.4}$$

The coordinates Y, Z are upslope and bottom normal with respect to the plane bottom that is inclined at an angle θ to the horizontal. $B(Y,Z,T) = -g(\overline{\rho} - \rho_0)/\rho_0$ is the mean buoyancy in terms of the mean density $\overline{\rho}(Z,T)$ and a reference density

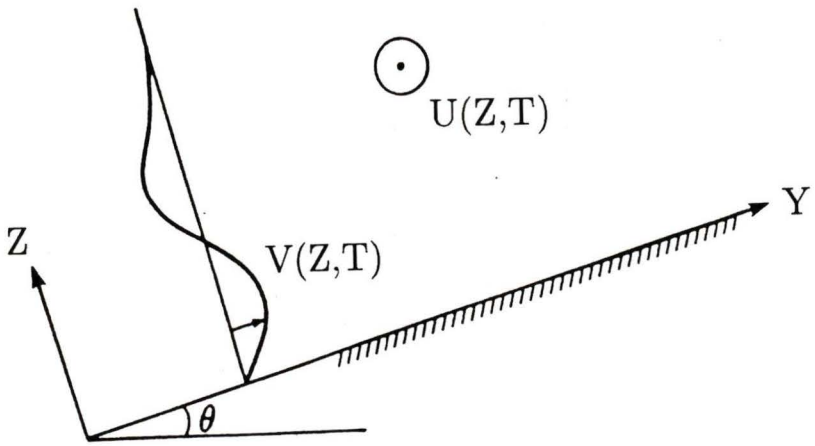

Figure 2.1: Definition sketch of the area under consideration.

ρ_0, and N^2 is the (constant) vertical buoyancy gradient in the interior of the fluid away from the slope. For flat interior isopycnals we must have:

$$\partial B/\partial Z \rightarrow N^2 \cos\theta \qquad \text{as } Z \rightarrow \infty \tag{2.5}$$

whereas

$$\partial B/\partial Y = N^2 \sin\theta \qquad \text{for all } Z. \tag{2.6}$$

The mean pressure $\overline{P}$ is taken with respect to the pressure in a fluid of density ρ_0 at rest. Eddy transports of X and Y momentum normal to the slope are represented in terms of the same eddy viscosity $\nu(Z,T)$ which represents the ratio of momentum flux to mean gradient. The eddy buoyancy transport normal to the slope is parameterized in terms of an eddy diffusivity κ . The Coriolis parameter $f = 2\Omega \sin\alpha$, where Ω is the component of the earth's rotation rate normal to the bottom, and α is the latitude. Use of this parameterization necessarily restricts the applicability away from equatorial regimes, and a mid-latitude α shall be assumed.

In general, values will be presented appropriately scaled by canonical values so units are not at issue, but the convention that dimensional values will be upper case, and nondimensional values lower case, will be adopted.

Elimination of $\overline{P}$ from equations 2.1 to 2.4 leads to 3 coupled equations in U, V and perturbation density $B' = B - N^2(Y \sin\theta + Z\cos\theta)$. These equations are independent of Y and can be nondimensionalized in terms of a height scale $H, (Z = Hz)$, a timescale $f^{-1}, (T = f^{-1}t)$, and a buoyancy scale $B' = fN^2 \cos\theta b'$.

Velocities are scaled $(U, V) = fH \cot\theta(u, v)$. This yields a set of equations in terms of a slope Burger number $S = N^2 \sin^2\theta/f^2$, an Ekman number $E = \nu/(fH^2)$, and an eddy Prandtl number $Pr = \nu/\kappa$. These equations are derived in Appendix A, and are:

$$\frac{\partial u}{\partial t} - v = -\frac{\partial p}{\partial x} + E\frac{\partial}{\partial z}\left(\nu'\frac{\partial u}{\partial z}\right) \tag{2.7}$$

$$\frac{\partial v}{\partial t} + u - u_e = +Sb' + E\frac{\partial}{\partial z}\left(\nu'\frac{\partial v}{\partial z}\right) + F(u_e, u_0) \tag{2.8}$$

$$\frac{\partial b'}{\partial t} + v = E/Pr(\frac{\partial}{\partial z}\left(\nu'\frac{\partial b'}{\partial z}\right) + \frac{\partial \nu'}{\partial z}) \tag{2.9}$$

ν' is the nondimensional viscosity, $u_e = u_e(t)$ is the interior alongslope flow; and $u_0 = u_e(0)$. $F(u_e)$ is a function of the alongslope flow dependent on the form of the boundary conditions. Equation 2.9 assumes that in all cases, the forms of $\nu'(z)$ and $\kappa'(z)$ are the same. They differ only in a multiplicative constant, the Prandtl number.

The boundary conditions for u, v and b' will depend on the form of the assumptions made about the far field and will be given in each case. The exception to this is that the insulating boundary condition is assumed for b'. Total buoyancy $b = b' + z$, so $\frac{\partial b'(0)}{\partial z} = -1$ at $z = 0$. In this way it is always assumed that the fluid at the lower boundary has no mass flux.

2.1 Numerical Implementation

In equations 2.7 to 2.9, the Coriolis terms are integrated using a semi-implicit scheme. Following Roache [21], the diffusive terms are separated into two parts

and integrated separately.

$$\frac{\partial}{\partial z}\left(A\frac{\partial B}{\partial z}\right) = \frac{\partial A}{\partial z}\frac{\partial B}{\partial z} + A\frac{\partial^2 B}{\partial z^2} \tag{2.10}$$

These and all other terms are integrated using a forward time, centered space (FTCS) treatment, with one exception. An exception to the FTCS method existed for one case where the form of the diffusivity and boundary conditions were 'well behaved' (only one gradient boundary condition), and a semi-implicit treatment of the diffusive terms was possible. This Crank-Nicholson scheme (again Roache [21]) was checked in a number of ways. Analytically the method was evaluated for stability and error amounts. In fact, all of the diffusive calculations were analyzed for instabilities and amounts of error. The analysis also yielded maximum time step values.

The Crank-Nicholson scheme was used for a case in which only the stationary state was desired. The final state was checked by repeating this case using purely finite difference FTCS methods. Additionally, for selected cases, the resolution was doubled. Other cases were then run in which the time step was halved at the original resolution to check the robustness of the final states. The Crank-Nicholson was further checked by using a fully implicit method. The final version of the code using Crank-Nicholson actually uses a combination of implicit and semi-implicit timesteps, since it is known that semi-implicit methods have neutral stability (again, Roache [21]).

Several numerical problems did arise and they will be discussed in the context of the particular applications to which they pertain. Appendix B contains a brief outline of the computer files generated, archival procedures, and a sample program.

Chapter 3

Time-Independent Coefficients of Eddy Viscosity

Thorpe [15] has solved equations 2.1 to 2.4 for the case of time and space independent coefficients of viscosity and diffusivity. The solution in the dimensionless space is

$$u = \frac{1}{qPr}(1 - e^{-qz}\cos qz) \tag{3.1}$$

$$v = 2qEPre^{-qz}\sin qz \tag{3.2}$$

$$b' = \frac{1}{q}e^{-qz}\cos qz \tag{3.3}$$

where $q = \frac{1}{\sqrt{2E}}(1 + SPr)^{\frac{1}{4}}$. $q^{-1} = h_t$ will be referred to as the Thorpe scale and represents the buoyancy boundary layer scale. several features of the Thorpe [15] solution are upslope flow and reduced stratification within the Thorpe scale.

As a first check on the numerical methodology, and to gain insight into the behaviour of the systems, the solution to equations 3.1 and 3.2 are plotted in figure 3.1 after integrating for 3000 f^{-1} time units. It is noted here that wherever a comparison to theory is made, the solid line style will be reserved for the theoretical curve (in this case, the solid line and the almost solid chain-dash line).

It is seen that the model is doing a very good job reproducing the theoretical predictions. The upslope movement near the boundary is also clearly seen in the

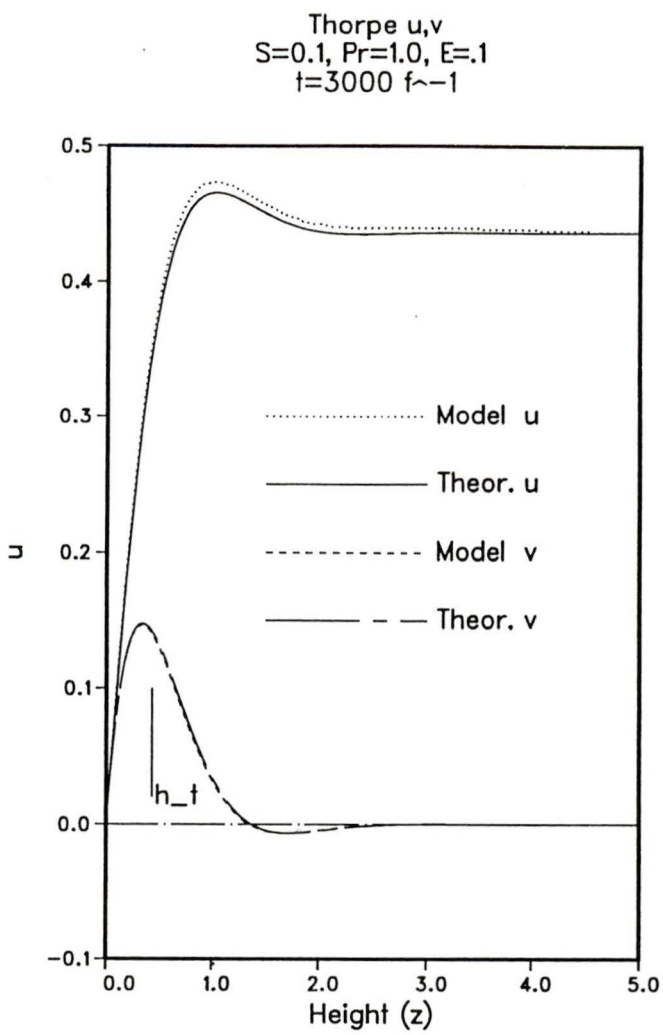

Figure 3.1: Model and theoretical profiles of u and v for the Thorpe solution. The Thorpe scale, h_t, is marked.

plots of v, as is the interior alongslope flow which is part of the solution (and hence serves as a boundary condition for the model).

Garrett [16], [17] recognized that one of the major drawbacks of the Thorpe [15] solution was that mixed layers will not, in general, have eddy coefficients which are the same in the whole fluid column, rather they will tend to be higher in the well mixed region. Garrett [16] has identified two regimes when the eddy coefficients are constant in time but variable in space over some scale h. With q based on ν and κ at $z = 0$, Garrett [17] shows that for values of qh which are small, the fluid is well mixed where mixing is strong so buoyancy forces are weak and boundary

mixing will not be very effective overall. If qh is large, however, buoyancy forces can restratify the fluid in the region where mixing is active and mixing effectiveness will be relatively high.

Garrett [17] has extended the analysis to cases where the eddy coefficients are constant in time but variable in space, and has established an analytic solution for a more physical case where the diffusivity is constant within the well-mixed layer, and zero outside. Before this case is considered, however, a test case at high qh with smoothly varying eddy coefficients will be considered.

3.1 Low Ekman Number (high qh)

Consider a case at low Ekman number ($E << 1$) with time-independent eddy coefficients smoothly decreasing with distance from $z = 0$. In this case, qh is large and gradients may be considered smooth, such that second derivatives in z may be neglected. Assuming stationarity and no external forcing, time dependent terms and u_e can be neglected and equations 2.7 to 2.9 can be written:

$$-v = E\frac{\partial u}{\partial z}\frac{\partial \nu'}{\partial z} \tag{3.4}$$

$$u = Sb' + E\frac{\partial u}{\partial z}\frac{\partial \nu'}{\partial z} \tag{3.5}$$

$$v = E\,\mathrm{Pr}\left(\frac{\partial b'}{\partial z} + 1\right)\frac{\partial \nu'}{\partial z} \tag{3.6}$$

The second term on the right of equation 3.5 is neglected since it is much less than the other terms, so the solution becomes,

$$\frac{du}{dz} = -\frac{S}{1+SPr}, \quad v = E\frac{d\kappa'}{dz}\frac{SPr}{1+SPr}, \quad \frac{db'}{dz} = \frac{-1}{1+SPr} \tag{3.7}$$

An exponential profile of diffusivity $\nu'(z) = e^{-z}$ was used to test 3.7 for 2 values of S, E and Pr. The theoretical values were used as the boundary conditions in the

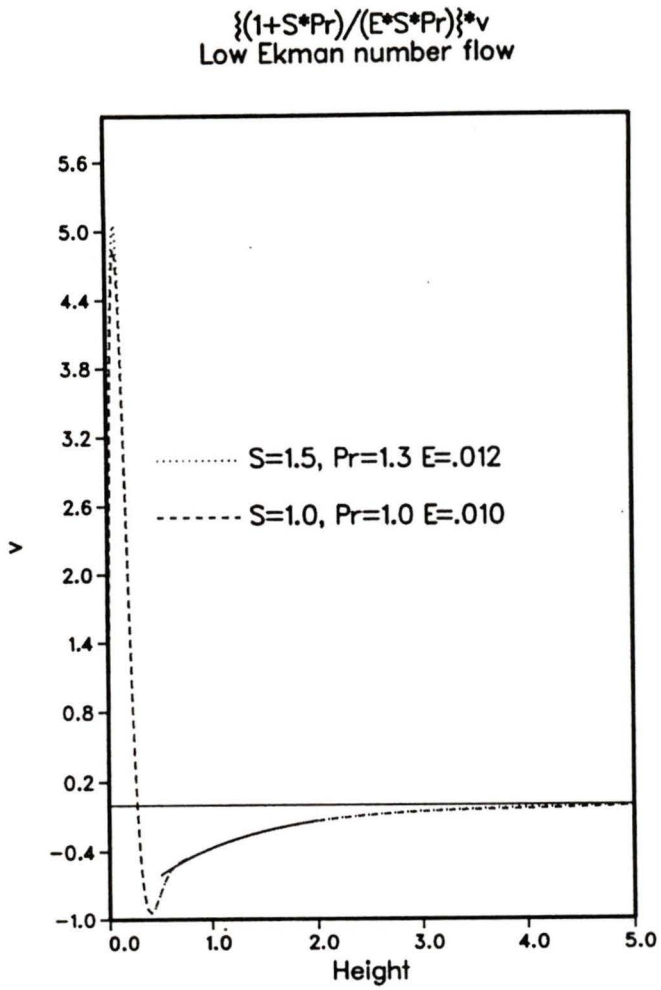

Figure 3.2: Profiles of v for two cases of Low Ekman number flow. The solid line is part of the theoretical solution.

far field and $u = v = 0$ at $z = 0$. Use of two gradient boundary conditions on b' precluded the use of Crank-Nicholson (Roache [21]) so FTCS was used.

Within a few tens of nondimensional timescales, the values of v versus height settled down to their theoretical values (Figure 3.2). On this figure, the values have been scaled by their theoretical values. Beginning at a height of .4, the theoretical prediction e^{-z} is plotted. A zero line is also plotted.

Shown on Figure 3.2 are the values of the parameters used for the test cases. It is seen that the scaled solutions for the two cases are very similar and agree with the theoretical prediction for nondimensional height scale, $h > .5$. The convergence

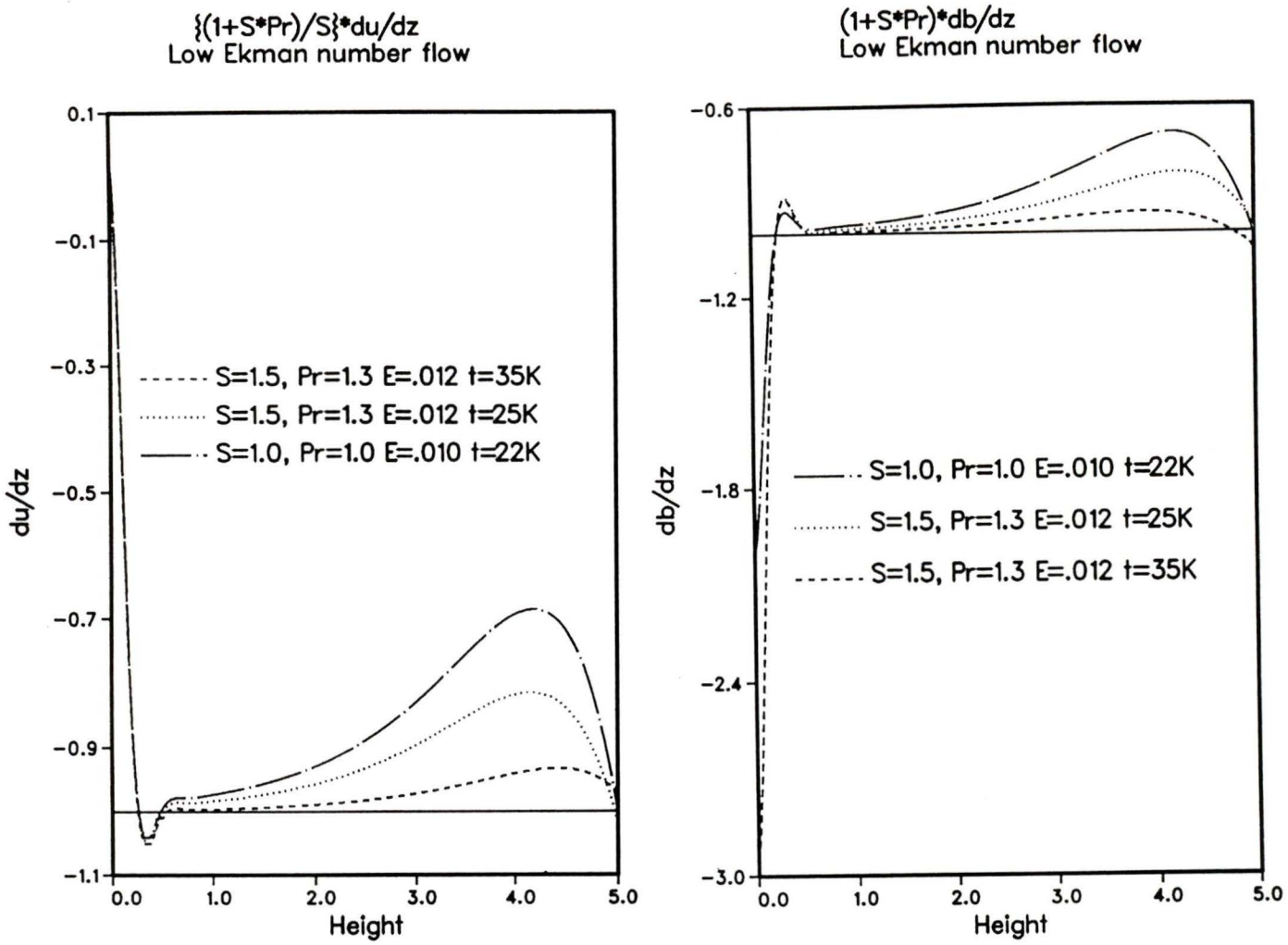

Figure 3.3: Profiles of (left) $\frac{du}{dz}$ and (right) $\frac{db'}{dz}$ for 2 cases of Low Ekman number flow

to the theoretical values for u and b' is much slower, of order 10^4 time units. This is to be expected, as Equations 3.7 show u and b' is of order 2.5 at $z = 5$ with S and Pr of order unity. With Ekman numbers of around .01 and $e^{-5} \approx .007$, this calculation yields a timescale for change at the top of the domain of about $3 \cdot 10^4$ time units.

Figure 3.3 shows gradients of u and b' scaled by their theoretical values for the same cases as Figure 3.3. The theoretical values are also plotted for reference. Values at two times are plotted for one of the cases.

This figure illustrates the slow convergence of the process, though the theoretical

values are approached. As expected, the convergence is greatest just above $z = .5$ where the diffusivity is greatest and the timescale of convergence is of order 10^4 time units. It must be mentioned that for these very long times, the values of u and b' are much greater than those of v, and the v profiles are subject to internal wave oscillations which eventually dominate the profiles due to their large magnitudes relative to the average values of v. The generation of these oscillations is associated with the slow convergence of the solution.

The diffusive damping of these oscillations is quite slow but they could be removed by a time filter. The oscillations do not affect the evolution of u and b', however and it is concluded that equations 3.7 are confirmed for the high qh case. It is also concluded that the code is verified for the more interesting cases to follow.

3.2 High Ekman Number (low qh)

3.2.1 Testing the Analytic Theory for Ideal Parameters

Garrett [17] has solved equations 2.1 to 2.4 for a very particular representation of eddy parameters which vary in space. A 'slab' model is considered in which $\nu(z)$ is high for $0 < z < h$, (ν_1) and low for $z > h$, (ν_2), with $qh << 1$ such that the water is well mixed for $0 < z < h$. It is also considered that $E = \infty$ in the well-mixed region. The solution is then defined in terms of $\epsilon = \nu_2/\nu_1 \rightarrow 0$ and a prediction for the velocity jump at the top of the high diffusivity region is obtained of

$$U_\infty = -\frac{3}{8} f H \cot\theta \frac{S}{(1 + SPr)} \tag{3.8}$$

Nondimensionally,

$$u_\infty = -\frac{3}{8} \frac{S}{(1 + SPr)} \tag{3.9}$$

where the ∞ indicates that $1/\epsilon$ has been set to infinity. Garrett [17] also gives a prediction for the jump in buoyancy, but to test the model, u will be used. There are, hence, 2 independent parameters which specify the problem, S and Pr.

Numerically, a jump in diffusivity exactly at $z = h$ is impossible, as is the constraint that $\epsilon = 0$ and $E = \infty$. For the purposes of testing equation 3.9, the following smooth analytic form of ν' is used:

$$\nu'(z) = \left(\frac{1+\epsilon}{2}\right) + \left(\frac{1-\epsilon}{2}\right) \tanh\left(\frac{h_0 - z}{\delta}\right) \tag{3.10}$$

where δ is a shaping parameter The form of equation 3.10 guarantees that $\nu'_1 = \nu'(0) = 1$ and $\nu'_2 = \nu'(\infty) = \epsilon$. The form of the diffusivity is also analytically tractable with continuous derivatives. E is taken to be 10, as this is large enough to make secondary terms in the Garrett [17] solution insignificant, but small enough to be capable of numerical integration.

By integrating the full model to stationarity using this form of the diffusivity, the values of ϵ and δ can be progressively reduced to approach the slab model. For this case, the Crank-Nicholson timestepping method was used and the interior flow allowed to adjust to the boundary mixing. The boundary conditions are, hence: $u(0) = v(0) = 0$, $\frac{\partial u(h_{max})}{\partial z} = \frac{\partial v(h_{max})}{\partial z} = 0$, $b'(h_{max}) = 0$, where h_{max} represents the top of the computational domain.

For all the simulations of this case, $h_0 = 1$. Figure 3.4 shows typical profiles of u, v and $b' + z$, where the nondimensional background gradient of buoyancy has been added for clarity. The buoyancy plot has also been scaled to fit on the page, and the vertical scale refers to nondimensional velocities. As a point of reference, if h_0 is $10m$, then the dimensional values of diffusivity for an Ekman number of 10 and $\epsilon = .001$ are $.1m^2/s$ and $10^{-4}m^2/s$, in the near and far fields respectively.

This particular case was run for 1500 f^{-1} timescales to reach stationarity. Figure 3.4 shows that the mixing extends slightly beyond h_0. Consistent with the Garrett [17] theory, the alongslope velocity is zero within the mixed layer and has a negative jump at the top of the interface which extends into the flow interior. Upslope velocities, v, are limited to the mixed region and the top of the interface. This plot also illustrates the difficulties in measuring the jump in b' as a test of the theory, compared to measuring u.

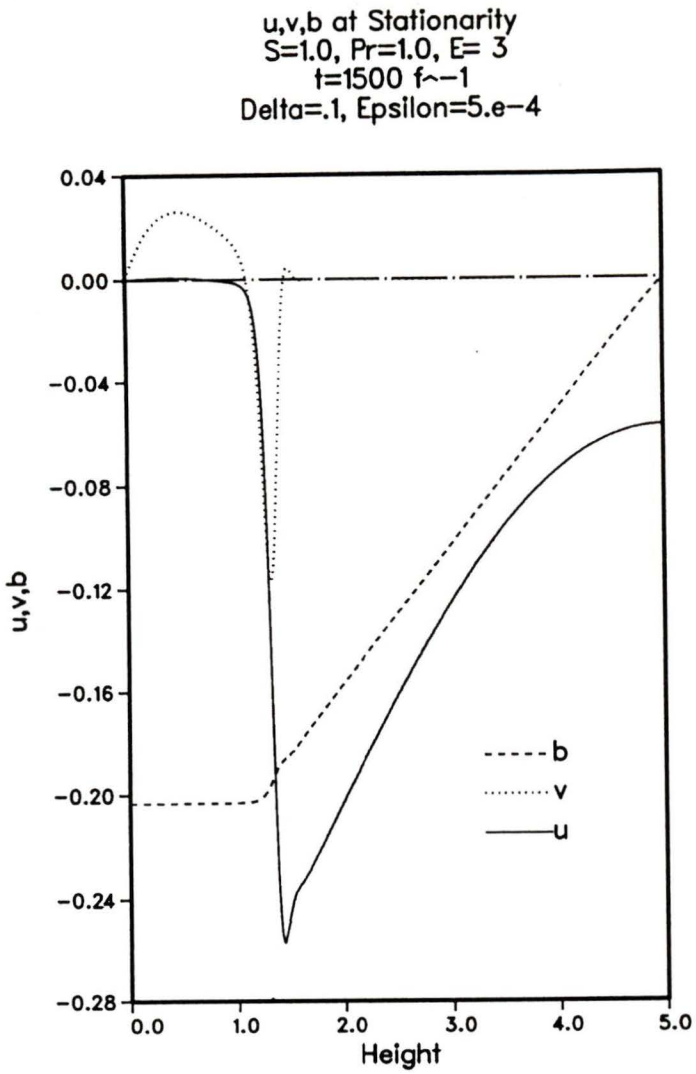

Figure 3.4: Typical profiles of u, v and b for a high Ekman number case.

Figure 3.5 illustrates the effect of altering the values of ϵ and δ on the profiles of u. For these cases, $S = 1, E = 10$ and $Pr = 1$, and it is seen that as δ is made smaller at constant ϵ (Figure 3.5 left), the jump moves closer to $h_0 = 1$. The values of u are scaled by u_∞ and it is seen that the values of the scaled u jump are greater than u_∞ for $\delta = .1$ and less for $\delta = .025$.

Figure 3.5 (right) also shows that as ϵ is reduced at constant δ, the velocity jump increases and again brackets u_∞, but interestingly, the value at $z = 5$ is fairly constant.

By determining the maximum values of u from large numbers of simulations at constant S, Pr and E, a test of the slab theory is now possible. Figure 3.6 shows

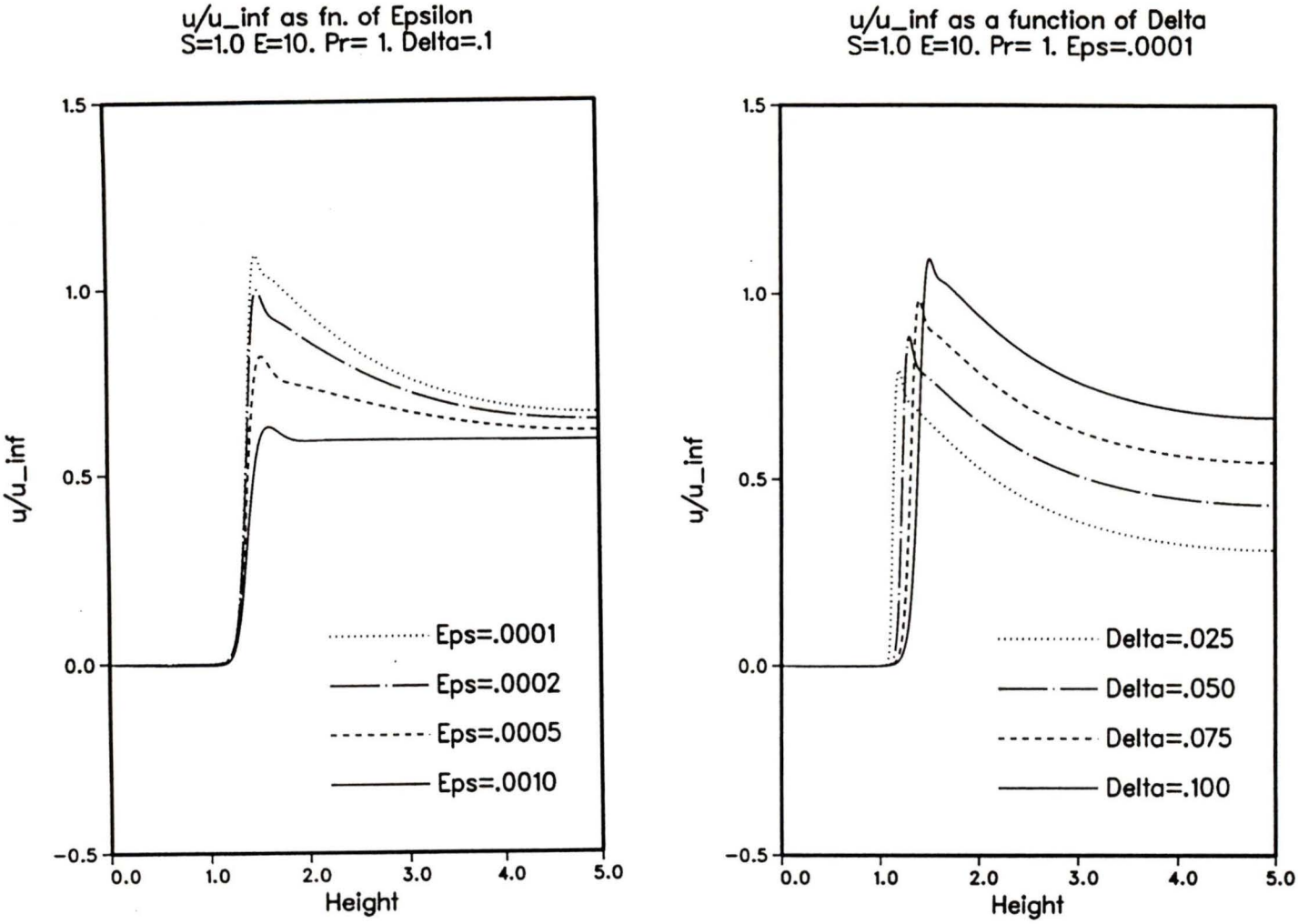

Figure 3.5: The effect of altering δ and ϵ on the profiles of u

(left) the values of u/u_∞ for a sample case plotted as functions of ϵ, and producing the highest order possible (third order) polynomial fits (Press *et al* [22]) for various values of δ. These simulations were all run to stationarity for times which varied approximately inversely as E and ϵ, which is a representation of the time needed for effects generated at the interface to diffuse to the upper boundary.

The $\epsilon = 0$ intercepts from the polynomial fits were then plotted as functions of δ (Figure 3.6, right). Numerical difficulties prevented smaller values of δ being simulated (the grid spacing must shrink as δ is reduced), but it is seen that the u jump does tend to u_∞ as both δ and ϵ are reduced to zero. On Figure 3.6, right, a quadratic has been plotted between $(0, 1)$ and $(.1, 1.22)$. In fact, there

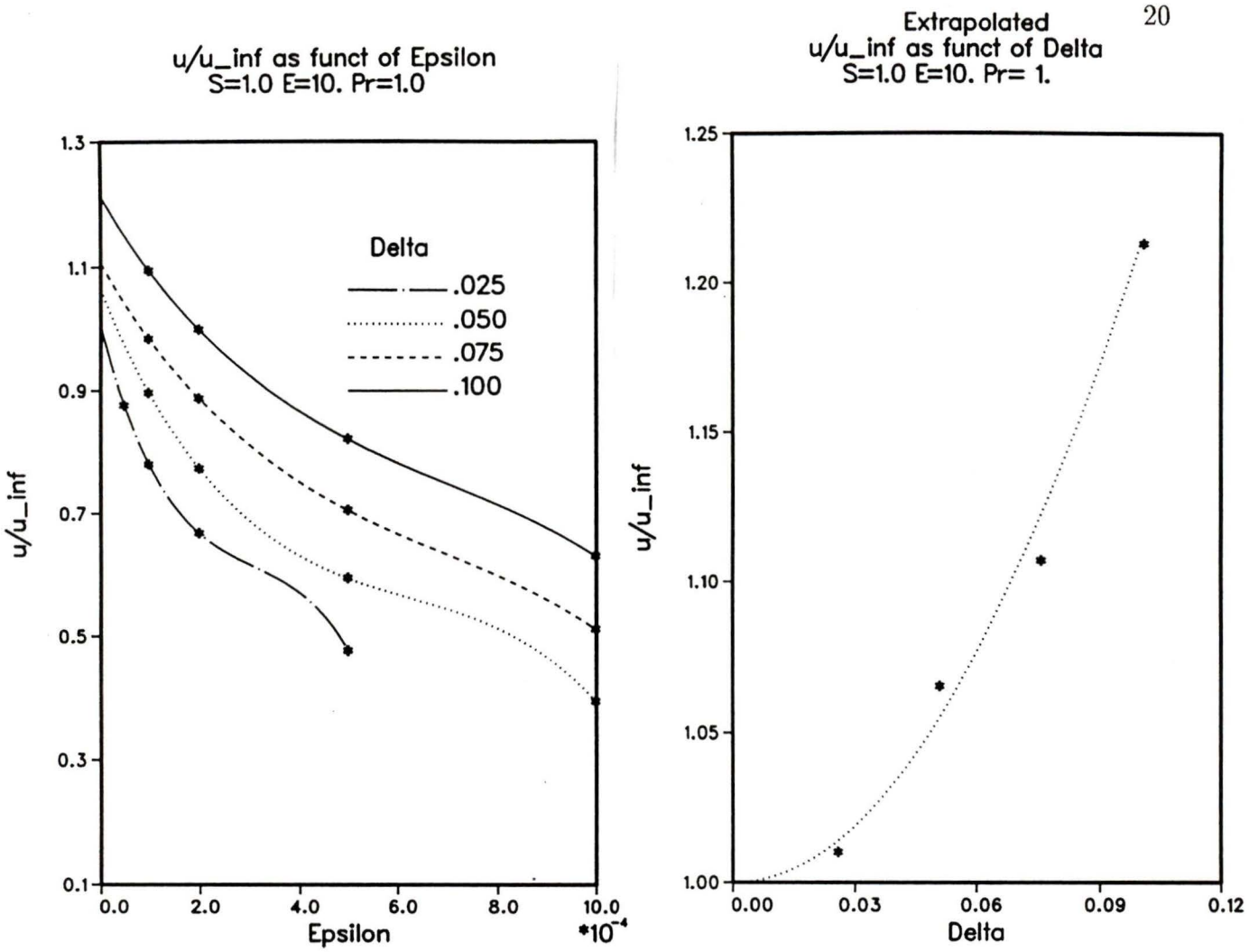

Figure 3.6: (Left) Measured (*) and fitted (line) u/u_∞ as a function of ϵ for various values of δ. (Right) The $\epsilon = 0$ intercepts of the fitted lines plotted as a function of δ.

is no compelling reason for producing such a plot except to emphasize that the theoretical prediction is not unreasonable. Generation of these extrapolations of extrapolations is not an exact science, but the Garrett [17] result is approached as the ideal parameters are approximated.

It is concluded that the Garrett [17] theory for the slab model is verified even though the Ekman number is not infinite as the theory requires.

3.2.2 Error Behaviour for Other Parameters

The case reported in the previous section is taken as a representative run and other cases have been run in which S, Pr and E have been varied to gain insight into the applicability of the theoretical solution. Table 3.1 lists the parameters used.

Description	S	Pr	E	Figure
Basic Run	1	1	10	3.6
Lower S	.5	1	10	3.7
Lower S	.3	1	10	
Low Pr	1	.5	10	3.8
High Pr	1	2	10	

Table 3.1: Parameters for the High Ekman Number Simulations

Figures 3.7 and 3.8 show the values of u/u_∞ for the values in the table. Taken together, Figures 3.7 and 3.8 show that the theoretical solutions are approached as δ and ϵ are reduced. However, the velocity jump can acquire different values and even go negative for some parameterizations, particularly for lower values of the Burger number. Since the Thorpe solution has positive u, this tendency is perhaps not unexpected as the limit $\delta \to \infty$ is a Thorpe-like case.

Figures 3.6 and 3.7 indicate that the theory is better for larger values of S, though the intercept ($\epsilon = 0$) values are about the same. It must be emphasized that in these figures, the velocity jumps utilizing the simulations with the smallest values of ϵ and δ are suspect, and can make the zero intercepts of u/u_∞ overshoot the theoretical value.

Figure 3.8 indicates that the theory does better with larger Prandtl numbers, but the intercept values are about equal. In any event, the prediction of the Garrett [17] theory degrades when the interface between the well-mixed and non-mixed regions is non-slab like, or the diffusivity in the far field is non-zero.

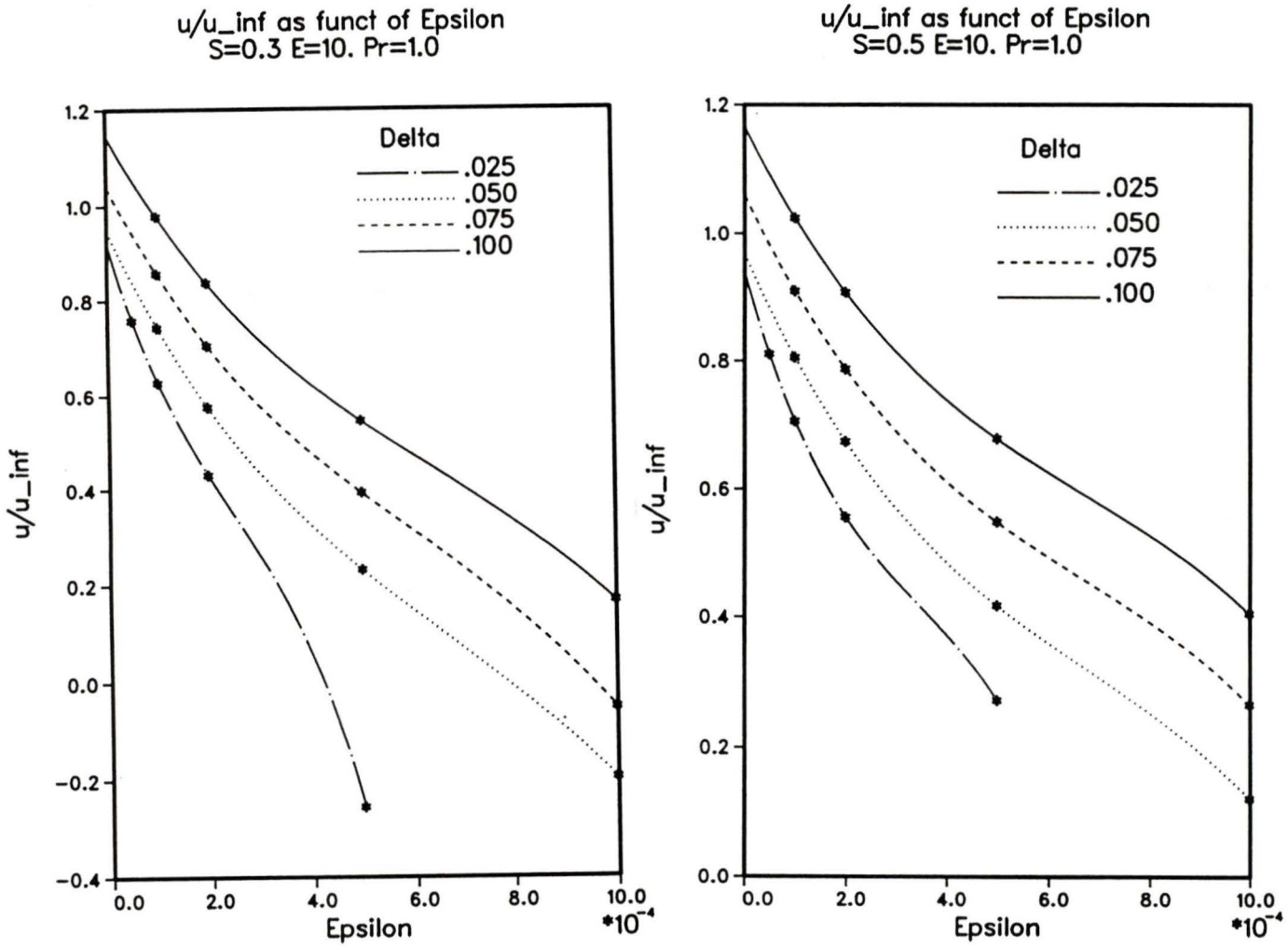

Figure 3.7: u/u_∞ for two values of the Burger number, (left) $S = .3$, (right) $S = .5$

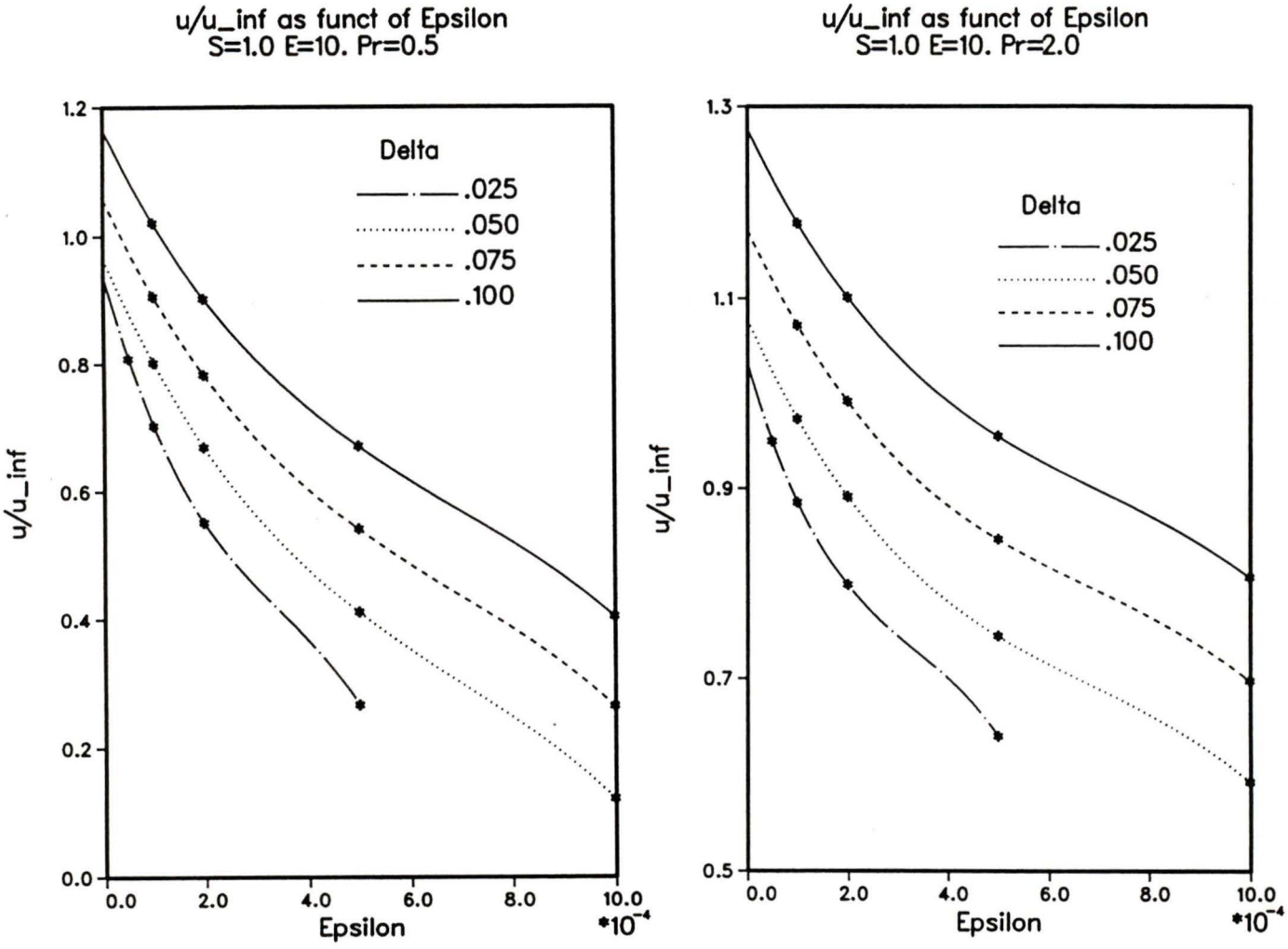

Figure 3.8: u/u_∞ for two values of the Prandtl number, (left) $Pr = .5$, (right) $Pr = 2$

Chapter 4

The Physics of Ekman Layer Shutdown

4.1 Basic Concepts and Model Development

Consider a uniform horizontal flow at right angles to a bottom slope. Standard Ekman theory predicts a net upslope or downslope movement of water. If the water is stratified, this transport will create a buoyancy force which will oppose the up or downslope movement of water and the Ekman layer will 'shutdown'. A ramification of this transport is that the upslope velocity must go to zero when the buoyancy force is strong enough. There is no subsequent spin-down of the fluid column due to bottom friction. The boundary current will continue to flow as if the boundary had no friction at all. MR92 refer to this process as a 'slippery' boundary and use it to explain the penetration of the Greenland current far beyond what Ekman layer theory would predict. A more probable cause is that the tilted isopycnals associated with the current possess a great deal of potential energy (GMR) and can convert it to kinetic energy, thus maintaining the current against Ekman spindown.

There are other ramifications to this effect. If the alongslope flow is slowly time varying, then, as shown by MR92 and TL, the response during the upwelling favourable part of the cycle will be different than the response during the down-

welling part of the cycle.

This asymmetry has interesting implications for the whole cycle in terms of net mixing and steady states. The asymmetry results from the fact that on the upwelling part of the cycle, it is assumed that the isopycnals are advected up the slope, and there is no further mixing. On the downwelling part of the cycle, however, the isopycnals are bent down allowing further mixing. This asymmetric response is described in detail in TL and figures of boundary layers and alongslope flow are presented which support this hypothesis.

The aim of this section is to extend the investigations of MR92 and TL to obtain a consistent theory of Ekman layer shutdown. The simplest model of the behaviour is illustrated by a constant interior flow, $u_e = u_0$ at $z = \infty$. Based on the previous studies, it is expected that the mixed layer will change in height for both positive and negative u_e, and the MR92 formulation of diffusivity based on a gradient Richardson number is adopted. The Richardson number is essentially a ratio of a turbulence timescale to a stability timescale, and there are good theoretical reasons (*e.g.* Howard [24]) why it is used as a signature of instability in a water column. Nondimensionally, it takes the form:

$$Ri = S(\frac{\partial b'}{\partial z} + 1)/\left((\frac{\partial u}{\partial z})^2 + (\frac{\partial v}{\partial z})^2\right) \tag{4.1}$$

Adopting the diffusivity as a function of Richardson number used by MR92: if $Ri < .2, \nu = \nu_1$, and if $Ri > .3, \nu = \nu_2$, with a linear ramp between $.2 < Ri < .3$ The choice of $Ri = .25$ as a mixing cutoff is probably good, but the values of ν_1 and ν_2 are somewhat arbitrary, as is the shape of the diffusivity function. TL adopted a different approach, assuming a fully mixed layer and a bulk Richardson number formulation from which they obtained the mixed layer height, h. They did not allow their mixed layer to become smaller, which precluded studies of thinning mixed layers (which is expected for upwelling favourable flows). TL integrated their model on the assumption of instantaneous response of u and v to h and then vice-versa without explicitly evaluating eddy coefficients.

For the bottom boundary condition, the bottom drag formulation of TL is adopted:

$$\nu \frac{\partial U}{\partial Z} = C_d |\boldsymbol{U}| U \tag{4.2}$$

where $|\boldsymbol{U}| = \sqrt{U^2 + V^2}$. Nondimensionally, for the u equation this becomes:

$$E\nu' \frac{\partial u}{\partial z} = C_d \frac{N}{f\sqrt{S}} |\boldsymbol{u}| u = \frac{D}{\sqrt{S}} |\boldsymbol{u}| u \tag{4.3}$$

with a similar equation for v and with $D = \frac{C_d N}{f}$. This formulation differs from MR92 who adopted $u = v = 0$ at $z = 0$. This assumption prevented them from scaling their results in terms of the model parameters and resulted in a 'draggy' boundary (Parker MacCready, [23]).

The conditions at $t = 0$ for all of the following simulations of this section are as follows. $F(u_e, u_0) = 0$, $u = u_0$ and $v = 0$ except at z=0, where Equation 4.3 is used and $b' = 0$ except at $z = 0$, where the insulating condition on b is used. $\nu_2 = 10^{-4} m^2/s$. The flow parameters are nondimensionalized assuming a height scale $H = 20m$. The upper boundary conditions are $u = u_0, v = 0$ and $b' = 0$ for all times.

The code for this section was checked by repeating the simulations reported by MR92 using their bottom boundary conditions and verifying the bottom drag law formulation independently by qualitatively repeating one of the cases shown by TL using the Richardson number mixing assumption.

There are some numerical difficulties associated with the integration of equations 2.7 to 2.9 for the diffusivity and drag equations above. This is illustrated in the following figures. Four cases were integrated from $t = 0$ to $t = 1$ utilizing the same flow parameters ($S = .12, u_0 = .5, Pr = 1$), integrated over a domain of 1001 points from $z = 0, 2.5$. The only difference was that $D = \frac{C_d N}{f}$ was successively reduced. Values of u and v are illustrated in Figure 4.1.

The most obvious change is (as expected) that larger values of D create better defined gradients of u and v on which the Richardson number is defined. Careful

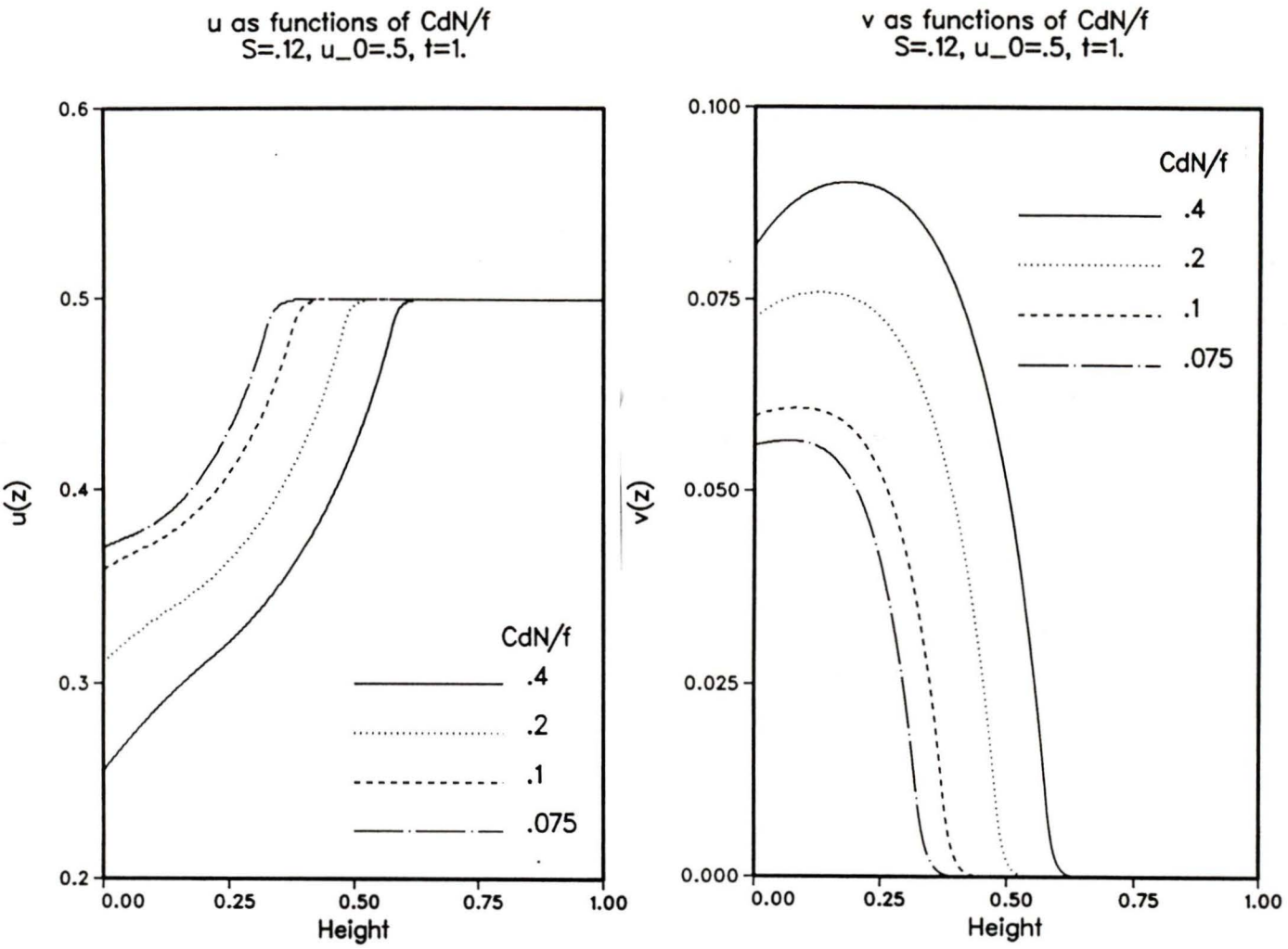

Figure 4.1: (Left) Profiles of u for successive values of $\frac{C_d N}{f}$ and the same flow parameters. (Right) same for v.

examination of Figure 4.1 shows some numerical 'jitter' beginning near $z = 0$ for the case of $D = .075$. At $D = .05$, the computer code generated numbers indicative of a numerical instability. Figure 4.2 shows profiles of perturbation buoyancy and diffusivity for the same cases as Figure 4.1. This figure indicates that the well-mixed region is squeezed into a smaller and smaller region as D is reduced.

Further examination of the problem has indicated that the code is generating diffusivity values at the boundary which oscillate between values near the minimum and maximum of the range. This creates problems for the calculation of $\frac{\partial \nu}{\partial z}$, as it is a centered difference operator. A $2\Delta z$ mode quickly develops.

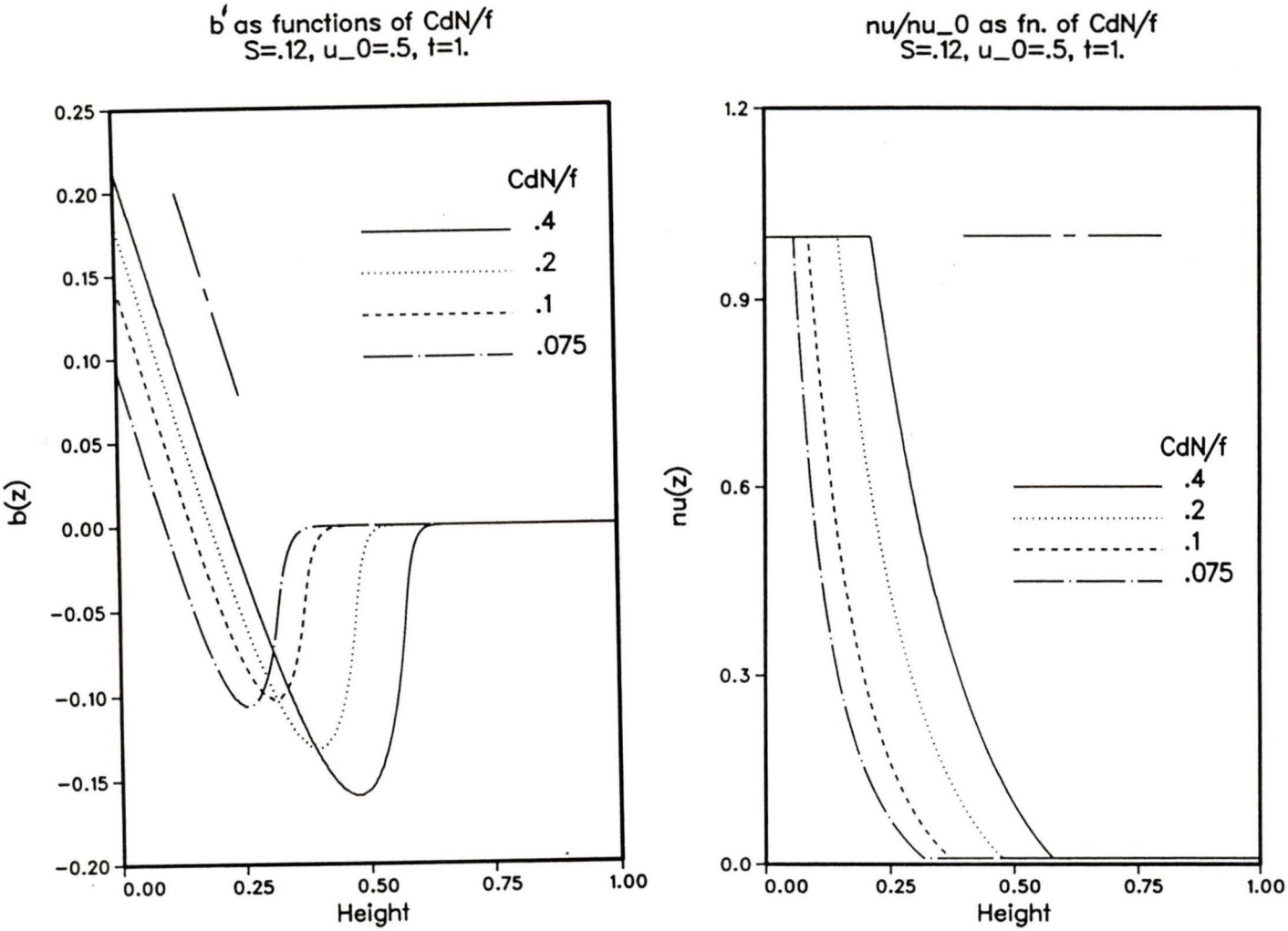

Figure 4.2: (Left). Profiles of b' plotted in the same manner as u. A -1 line is plotted for reference (perfectly mixed). (Right), Profile of ν scaled by the maximum value of ν plotted in the same manner as u.

This is not an advective timescale problem, and reducing the time step did not cure the problem. It can be cured through (doubling the) resolution, or by adopting an upstream definition of $\frac{\partial \nu}{\partial z}$.

$$\frac{\partial \nu}{\partial z} = (\nu(z + dz) - \nu(z))/dz \tag{4.4}$$

Use of this operator, however, implies a different set of equations are being solved as equation 4.4 can be written as:

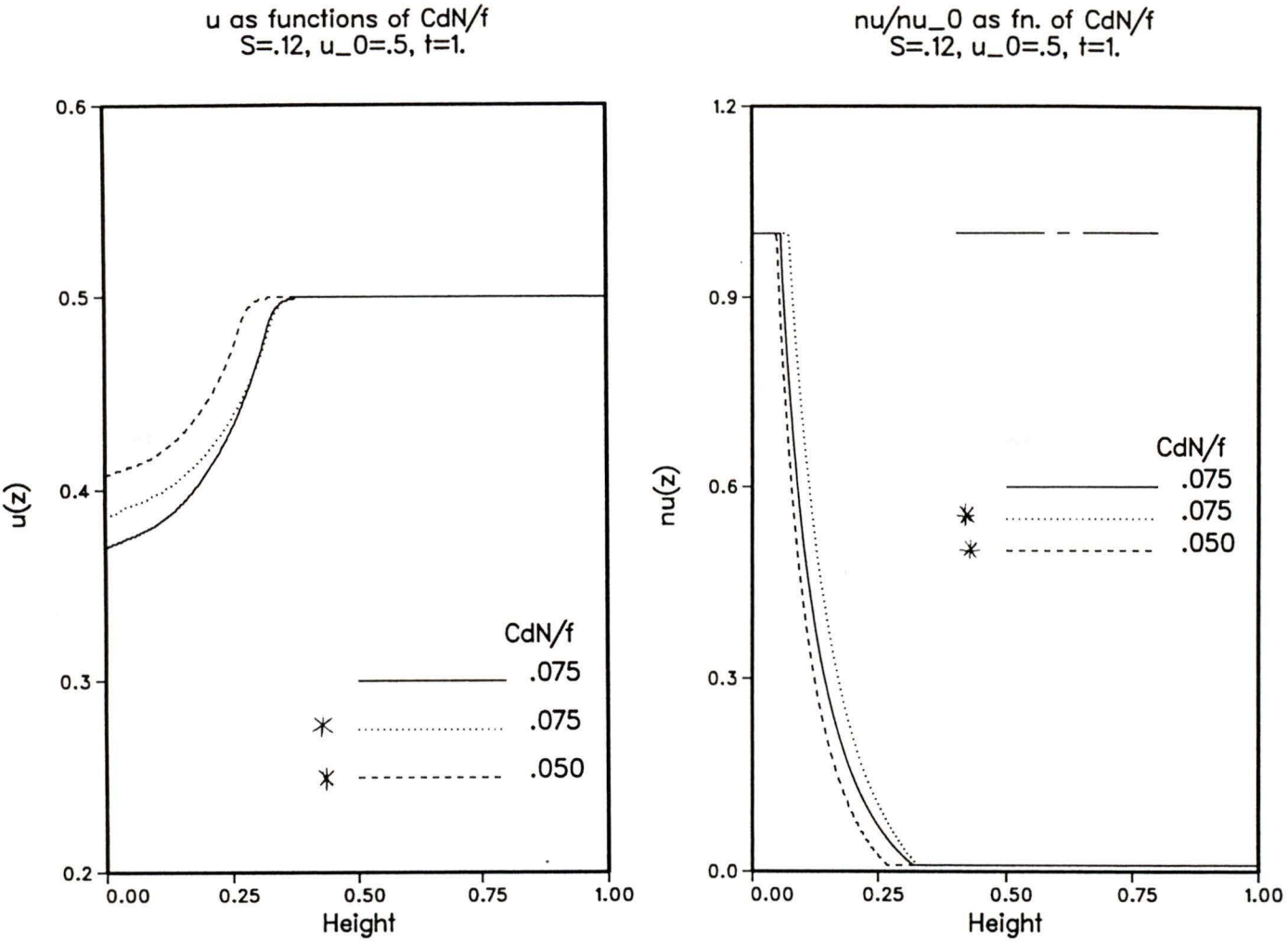

Figure 4.3: (Left). Profiles of u for two values of $\frac{C_d N}{f}$ and methods of calculating $\frac{\partial \nu}{\partial z}$. (Right), same for ν'. The asterisks denote cases using the upstream definition.

$$(\nu(z+dz)-\nu(z))/dz = (\nu(z+dz)-\nu(z-dz))/2dz+(\nu(z+dz)+\nu(z-dz)-2\nu(z))/2dz \tag{4.5}$$

which acts as a sum of a centered operator and a forcing term on u, v or b'.

Figure 4.3 shows the results of three simulations, two of which were run using the upstream definition of $\frac{\partial \nu}{\partial z}$. As is seen in figure 4.3, a price is paid for being able to simulate $\frac{C_d N}{f} = .05$ in that there is less mixing observed, and any numerical results using this definition would be suspect. MR92 avoided the problem by adopting a zero flow boundary condition which gives well developed shear at $z = 0$. TL

avoided the problem by adopting the bulk Richardson number formulation and a fully mixed boundary layer. The ultimate solution to the instability is probably to adopt logarithmic coordinates near the boundary, as described by Weatherly and Martin [25]. In this way, the whole boundary layer (commonly called the log layer due to it's logarithmic velocity profile) is explicitly modeled, rather than just the top of the layer.

In any event, this instability creates three problems:

1. Certain combinations of parameters in this section are not capable of numerical integration.

2. As simulations evolve in time, the velocities at the top of the boundary layer relax to zero (the desired effect), and then the numerical instability sometimes emerges.

3. Numerical regimes in which the external forcing varies in time (next section) are very susceptible as u_e goes to zero in parts of the forcing cycle.

We leave this section with reasonable confidence that the numerical methodology developed is believable, but still without a clear idea of how to extend the parameter regime of the time dependent forcing section ahead or carry out these cases to full shutdown.

4.1.1 Initial Layer Formation

The work of Pollard, Rhines and Thompson [26] and Thompson [27], indicates that the water near the boundary will mix to an initial height h_p in a time f^{-1},

$$h_p = \left(\frac{2\beta}{1+\beta}\right)^{\frac{1}{2}} u_i/\sqrt{S} \tag{4.6}$$

where $\beta = D/\sqrt{2}$, and u_i is the value of the far field velocity (in the present case, the alongslope velocity). Note that θ has entered equation 4.6 (through S) purely

as a consequence of the nondimensionalization. In fact, the scale is derived for flat bottoms.

The scale of equation 4.6 is derived from a bulk Richardson number formulation and assumes that momentum and density are well mixed. For the present formulation this assumption is not necessary. Equation 4.6 will be used, however, as an order of magnitude estimate in the following section. The issue of initial layer formation will be examined in more detail for the upwelling favorable flows where it is more critical.

4.2 Downwelling Favourable Flows

For the cases of downwelling favourable flows, ν_1 was chosen to be $10^{-2}m^2/s$, the value used by MR92. The model was integrated forward in time from the initial conditions. Figures 4.4 and 4.5 show profiles of u, v, b and ν' for a typical case run to $70f^{-1}$ time units.

It is seen that as time progresses, u at the boundary is brought to zero by an approximately linear slope which is constant in magnitude at all times. b also possesses a constant slope, and grows approximately to the same extent as u. The integrated upslope transport, v, is gradually reduced to zero as time progresses. MR92 and TL observed qualitatively similar results for their simulations. It is interesting to note that v develops a positive component near the boundary. This tendency is consistent with the Thorpe [15] solution for constant coefficients and probably represents the asymptotic state.

Figure 4.5 indicates that ν' is not constant, however, either in space or time. In fact, ν' appears to go to the minimum value of ν' at longer times. There was some worry that the upper boundary was not far enough removed and it was interfering with the evolution of the mixed layer, but subsequent plots (not shown) reveal that the effect is independent of the placement of the upper boundary. This 'collapse' of ν' was not observed by MR92, but it is possible that they did not take their simulation far enough given the 'dragginess' of their boundary.

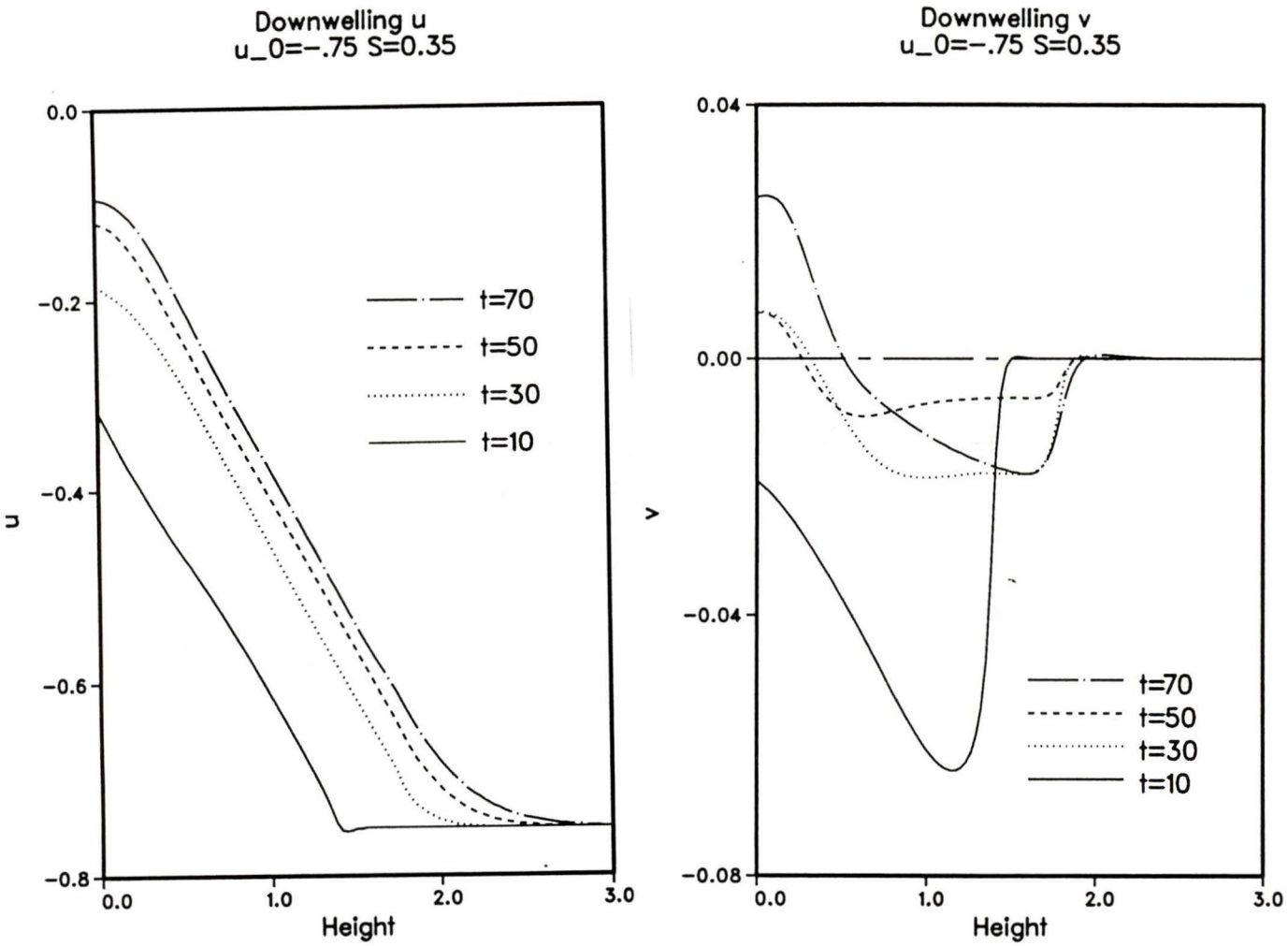

Figure 4.4: Typical time profiles of u and v for downwelling favourable flow.

4.2.1 A Model of Shutdown for Downwelling Favourable Flows

TL justified their neglect of the time dependent terms in the momentum equations on the grounds that there was an approximate equilibrium at all times between u, v and b'. Figures 4.4 and 4.5 indicate that this neglect may be a good approximation and, accordingly, the time dependency and diffusion terms can be neglected from Equation 2.8 to yield a thermal wind balance:

$$\frac{\partial u}{\partial z} = S\frac{\partial b'}{\partial z} \tag{4.7}$$

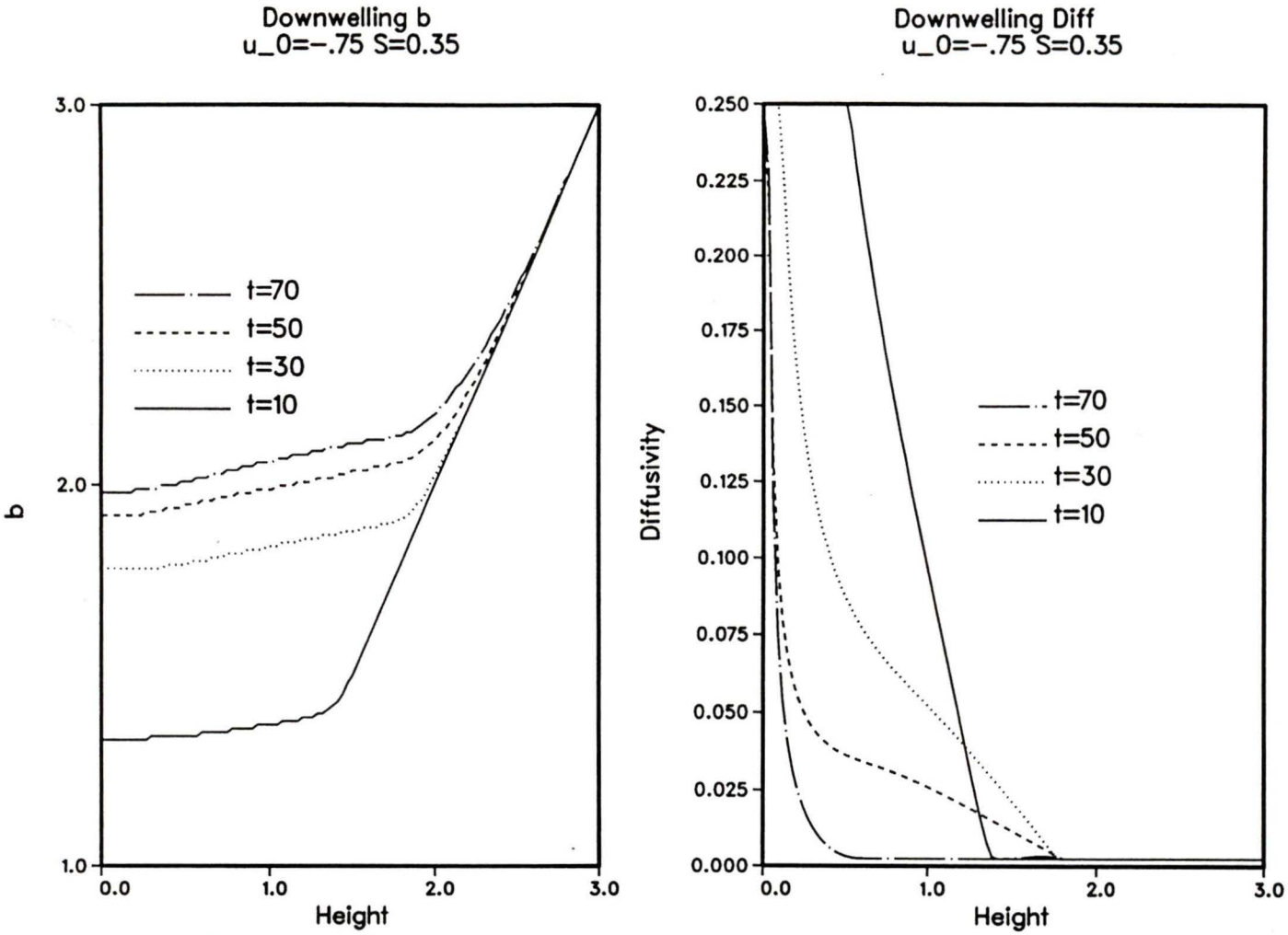

Figure 4.5: Typical time profiles of b and ν' for downwelling favourable flow.

Weatherly and Martin [25] cite evidence for such behaviour in the ocean. Combining this with Equation 4.1, and assuming the gradient Richardson number is $\approx \frac{1}{4}$ yields:

$$\frac{\partial u}{\partial z} = S(1 - S/4), \quad \frac{\partial b}{\partial z} = S/4 \tag{4.8}$$

Figure 4.6 shows that this is indeed true for $t > 10f^{-1}$ nondimensional time units. The theoretical values from Equation 4.8 have been plotted for reference. These are typical results, and other cases exhibited nearly identical behaviour.

It seems clear that the theory of continual slow mixing of the downwelled transport existing in thermal wind balance is a good one. With this relationship, a

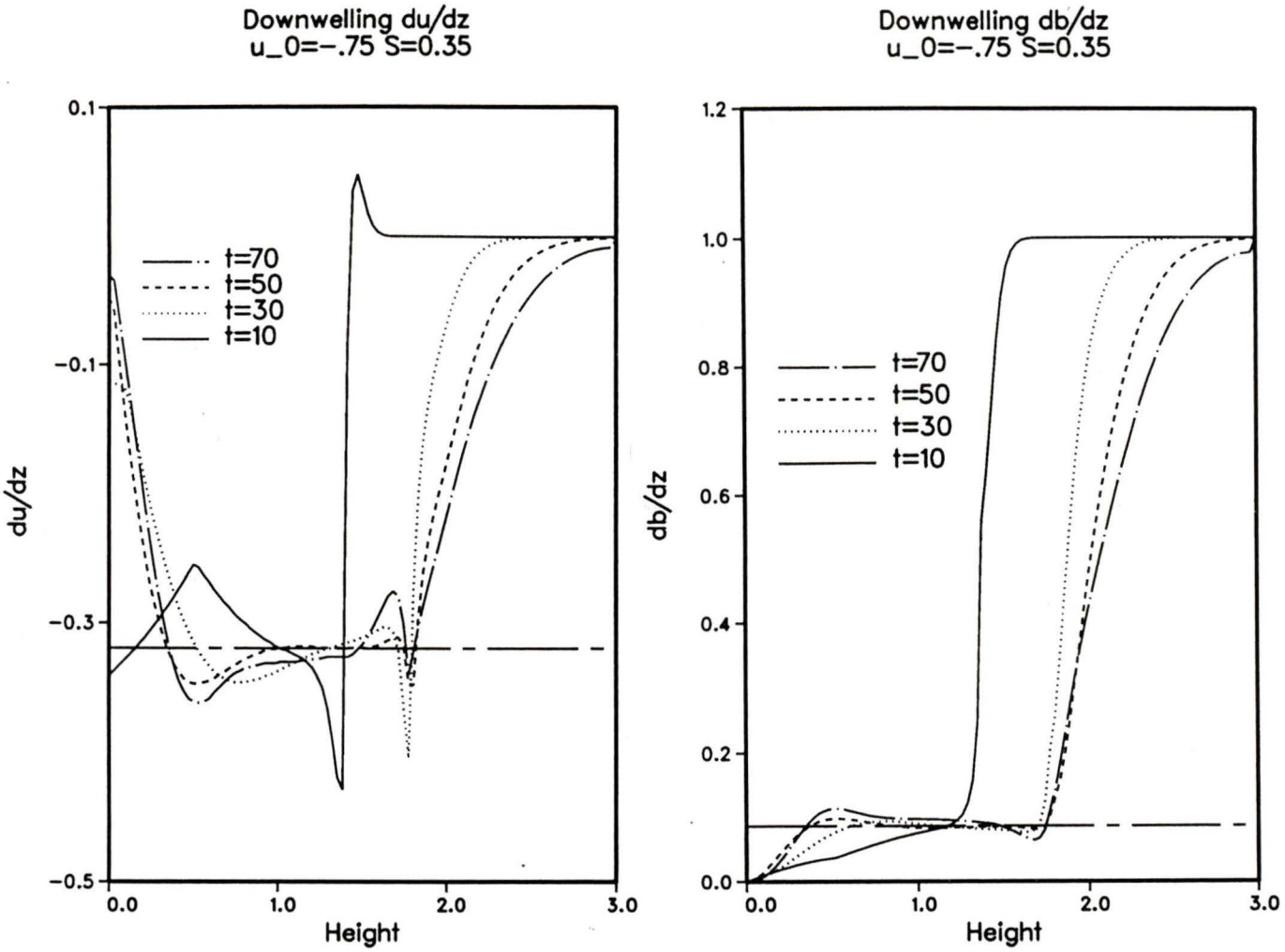

Figure 4.6: Typical profiles of (left) $\frac{\partial u}{\partial z}$ and (right) $\frac{\partial b}{\partial z}$ for downwelling favourable flow. The chain-dashed lines are the predicted slopes.

timescale for Ekman layer shutdown can be tested. If we ignore the initial scale of mixing, then the friction velocity (the value of u at the top of the log layer) is $u_f = u_0(1 - Sh)$, where h is the thickness of the thermal wind balance region. Assuming stationarity, equation 2.7 can be integrated with respect to z to yield the nondimensionalized Ekman transport:

$$Tr = \int_0^\infty v dz = \frac{C_d \frac{N}{f}}{\sqrt{S}} {u_f}^2 \tag{4.9}$$

With Tr_0 the transport at $t = 0$. For small S (as is likely), $\frac{\partial b'}{\partial z} \approx 1$. Equating the rate of change of buoyancy in a triangle of height h to the creation rate by the

Ekman flux against the y gradient of buoyancy:

$$\frac{d}{dt}\left(\frac{1}{2}h^2\right) = u_0^2 \frac{\frac{C_d N}{f}}{\sqrt{S}}(1 - Sh)^2 \tag{4.10}$$

This calculation is limited to small S to approximate a right angle triangle. Noting that the final height of the layer required to bring the friction velocity to rest will be about $h_d = u_0/S$, the substitution $Sh = h'$ yields:

$$h'\frac{dh'}{dt} = DS^{\frac{3}{2}}(1 - h')^2 \tag{4.11}$$

or letting $t' = DS^{\frac{3}{2}}t = t/t_0$:

$$\frac{h'dh'}{(1 - h')^2} = dt' \tag{4.12}$$

The time scaling is essentially that given by GMR. Equation 4.12 can be solved by separating into two parts, or writing as a power series, to yield t' as a function of h':

$$t' = \frac{1}{1 - h'} - \ln(1 - h') - 1 = \sum_{n=0}^{\infty} \frac{n+1}{n+2} h'^{n+2} \tag{4.13}$$

The simple theory developed above also predicts the friction velocity as $u/u_0 = (1 - h')$, transport $Tr/Tr_0 = (1 - h')^2$, and the integrated transport $\int_0^t Tr/Tr_0 dt'$. Four basic runs were performed for various run parameters and are listed in Table 4.1.

Label	S	$\frac{C_d N}{f}$	u_0	h_d/h_p	$t_0(f^{-1})$
A	.5	.25	-1.0	2.6	11.3
B	.35	.4	-.75	2.3	12.1
C	.2	1.4	-.5	2.5	8.0
D	.12	1.5	-1.0	2.8	16.

Table 4.1: Parameters for the Downwelling Cases

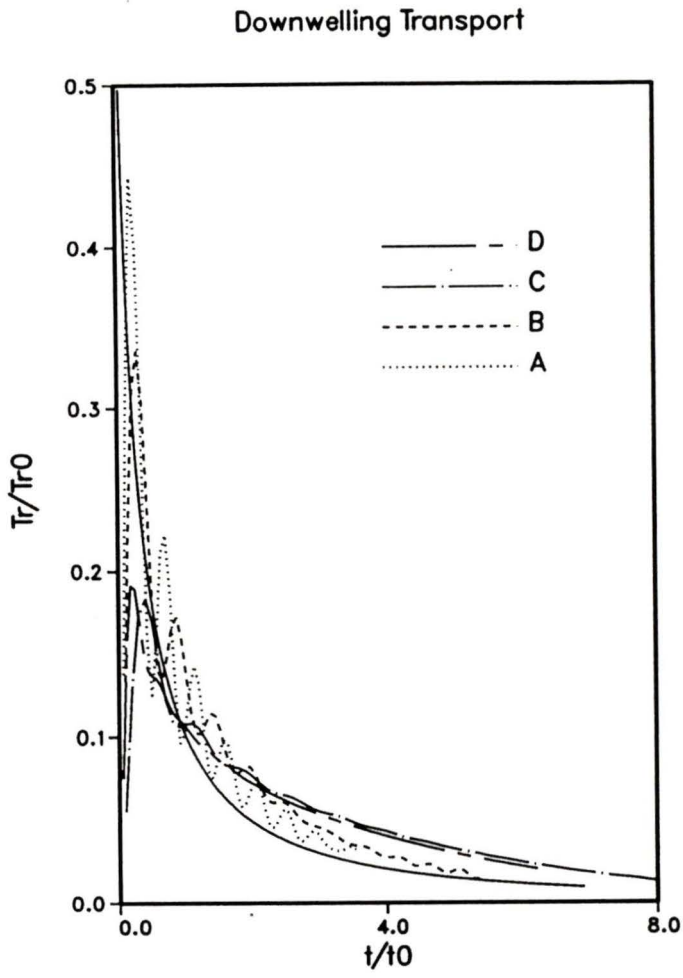

Figure 4.7: Scaled downwelling transport versus scaled time. The solid line is the theoretical prediction.

It is seen from Table 4.1 that the profiles were taken from case B. The ratios h_d/h_p are about the same for all cases.

Rather than try to estimate the height of the remixed water, the theory will be tested with the more objective measures of the friction velocity and (directly measured) integrated transport. Figure 4.7 shows the integrated Ekman transport. Despite the obvious oscillations, numerical results obey the shape of the 'universal' curve (solid) quite well after the initial mixed layer formation stage.

On Figure 4.7, it is also seen that the actual transport is less than the theoretical values during the initial phase, (about f^{-1}, Pollard, Rhines and Thompson, [26])

during which the initial mixed layer is evolving. After this, it is greater, indicating the theoretical prediction would probably be better if it were shifted by f^{-1} time units. Cases 'A' and 'B' follow the 'universal' curve better, and this is probably related to the lower values of $\frac{C_d N}{f}$ for these cases. The fifth column of Table 4.1 indicates that the ratios of predicted downwelling height to initial layer formation should not be the cause of cases 'C' and 'D' being worse. A simple calculation of the internal wave frequency ($= \sqrt{1+S}$) shows that the oscillations in the transport are at internal wave frequencies, as is expected.

As shown in Figure 4.8, this time asymmetry about the theoretical prediction is also reflected in the friction velocity, which is greater than the theoretical prediction after the initial phase.

In all cases, the friction velocity is very quickly reduced during the initial mixing phase, the degree probably dependent on $\frac{C_d N}{f}$. The evolution of u/u_0, however, appears to be independent of the parameters used, indicating that the time scaling is still correct, even if the details of the physics are not.

It is interesting that the transport agrees fairly well with the theory, whereas the friction velocity is less so. The integrated Ekman transport, Figure 4.9, follows the theoretical value, but is again playing 'catchup' due to the initial mixing time. A shift of f^{-1} would probably help here, also.

The curves in Figure 4.9 for lower values of $\frac{C_d N}{f}$ are clearly following the 'universal' curve better, but this could be misleading as S is also larger for these values. This is clearly related to the initial friction velocities and (obviously) transport being better, also. Gratifyingly, all integrated transport curves are approaching the value of $\frac{1}{2}$ which is the scaled area of the buoyancy triangles.

4.3 Upwelling Favourable Flows

The results of MR92 for upwelling favourable flows indicate that the water will mix to an initial height h_p given by Equation 4.6, followed by advection of the fluid up the slope until shutdown occurs. GMR have extended the analysis, assuming that a

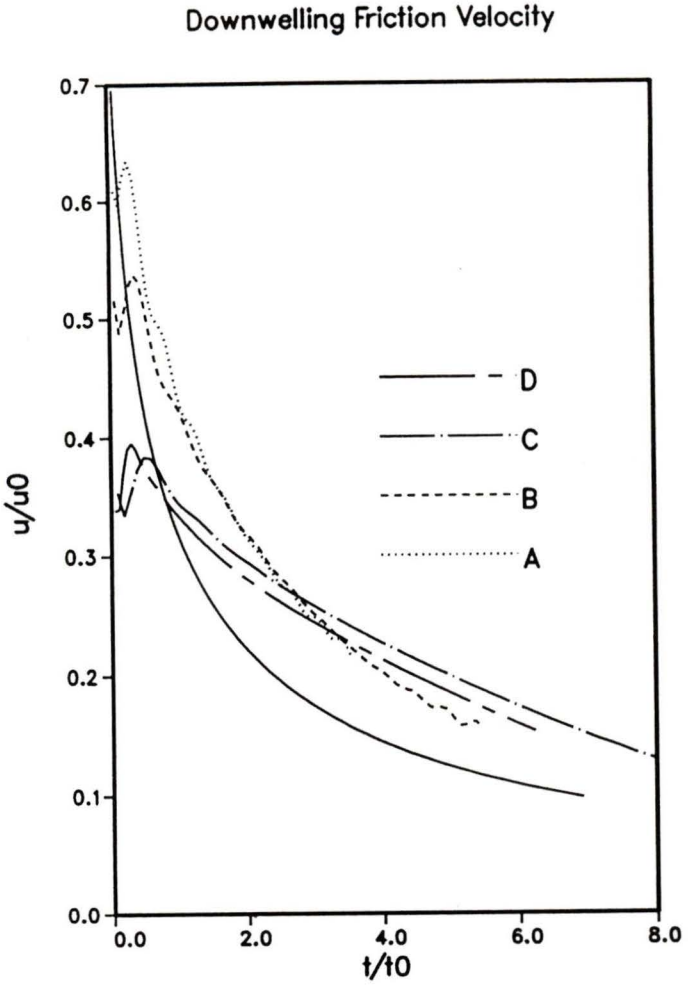

Figure 4.8: Scaled downwelling friction velocities versus scaled time. The solid line is the theoretical prediction.

thermal wind balance exists between b' and u over h_p. Before the theory is developed, however, it is necessary to return to the problem of initial layer formation.

4.3.1 Initial Layer Formation

MR92 used a value of diffusivity of $\nu_1 = 10^{-2} m^2/s$ in the well mixed region. This corresponds to a nondimensional value of $\nu_1' = .25$. This value is arbitrary. The Thorpe scale, q, yields a restratification scale. Does the fluid mix to the Pollard, Rhines and Thompson [26] scale, the Thorpe scale, or something entirely different? GMR produce a timescale of shutdown based on the Pollard, Rhines and Thompson

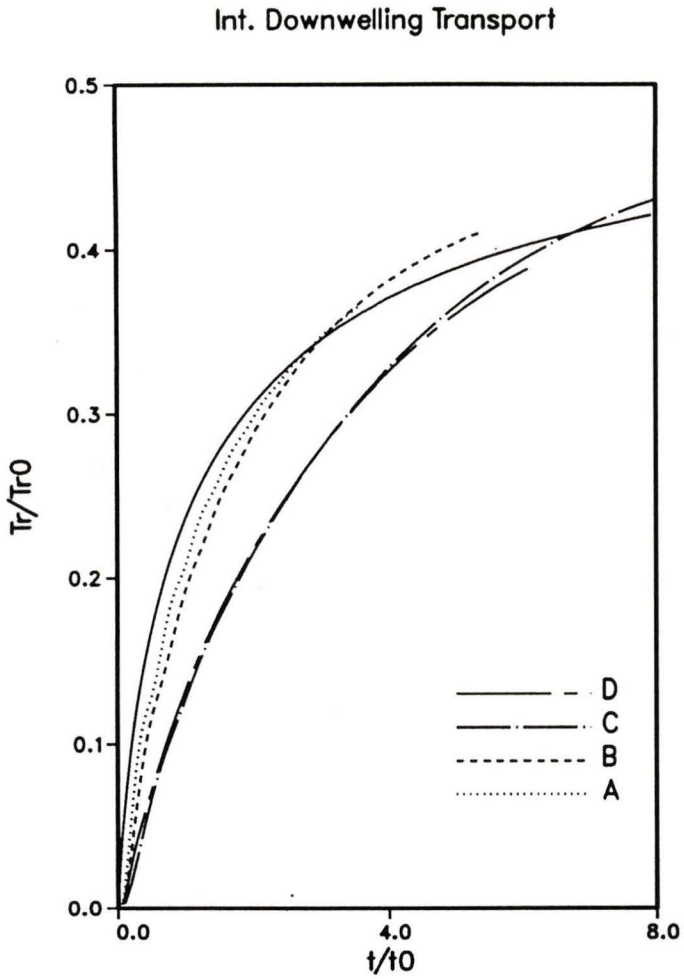

Figure 4.9: Scaled integrated downwelling transport versus scaled time. The solid line is the theoretical prediction.

[26] formulation and the intent here is to test this formulation which will be derived independently later.

Figure 4.10 shows the results of two cases, which were identical in every way except for the diffusivity; hence, they should have same initial mixed heights, according to the formulation of Pollard, Rhines and Thompson [26].

Figure 4.10 left, has a value of $h_t = .69$ and right, $h_t = 1.37$, and for both figures $h_p = .85$. Obviously, the Thorpe scale does matter, and hence, the simulations of the upwelling favourable flows will be run with ν_1' chosen so that the Thorpe scales and h_p are the same. This will not, however, guarantee initial mixed layer heights

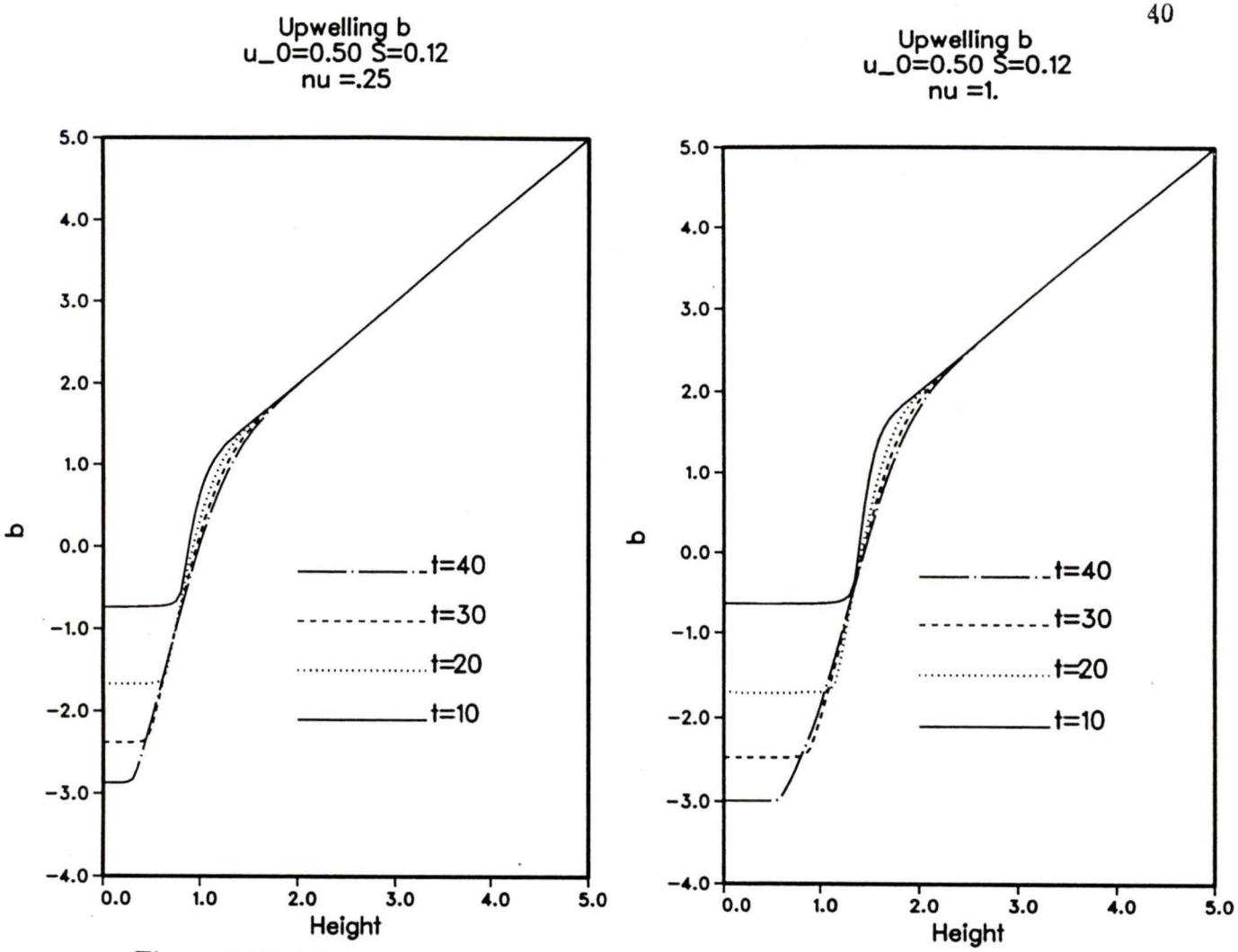

Figure 4.10: Time profiles of total buoyancy for 2 cases identical except for (left) $\nu_1' = .25$ and (right) $\nu_1' = 1$.

exactly equal to the predicted values, as we shall see.

4.4 The Theory of Shutdown for the Upwelling Cases

Based on the initial results of MR92, it is assumed that for upwelling favourable flows the water column will mix to an initial height h_p. Subsequent Ekman transport (with no further mixing) will eventually create a wedge of water which will be in thermal wind balance with no velocity at $z = 0$ and, hence, a velocity shear of u_0/h_p.

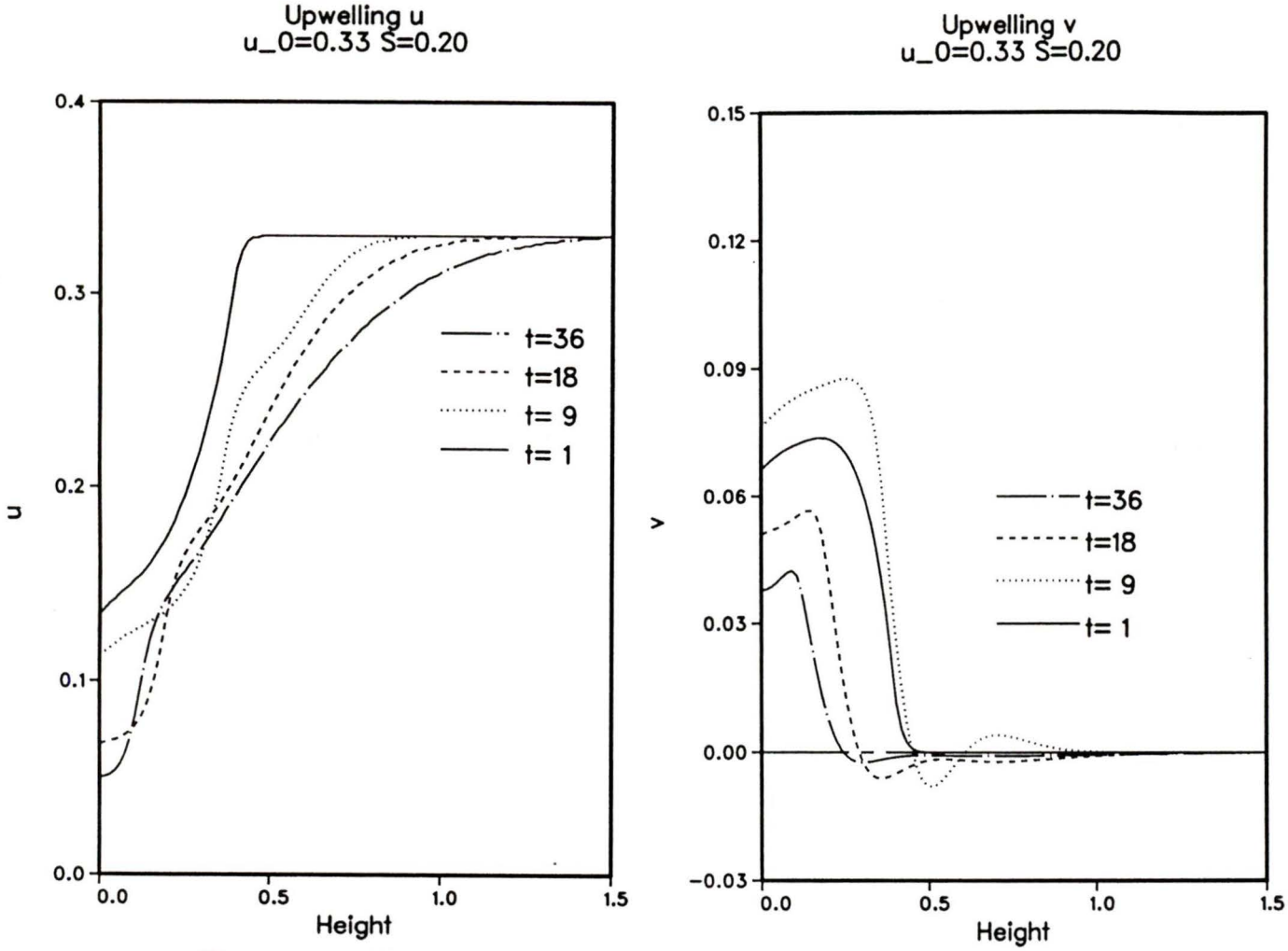

Figure 4.11: Typical time profiles of u and v for upwelling favourable flow.

In this theory, it is assumed that the initial slab is simply advected up the slope. If it is assumed that thermal wind balance (equation 4.7) is obeyed at all times, then a triangle argument can be made for the height of the mixed layer similar to that developed for the downwelling favourable case. For this case, Equation 4.12 is modified so that the time scaling is given by:

$$t = \frac{\sqrt{1+\beta}}{2^{\frac{1}{4}}} D^{-\frac{1}{2}} S^{-1} \tag{4.14}$$

This is essentially the same timescale given by GMR except for the correction when β (i.e. $\frac{C_d N}{f}$) is not much less than 1.

Figures 4.11 and 4.12 show time profiles of u, v, b and ν' for a typical upwelling

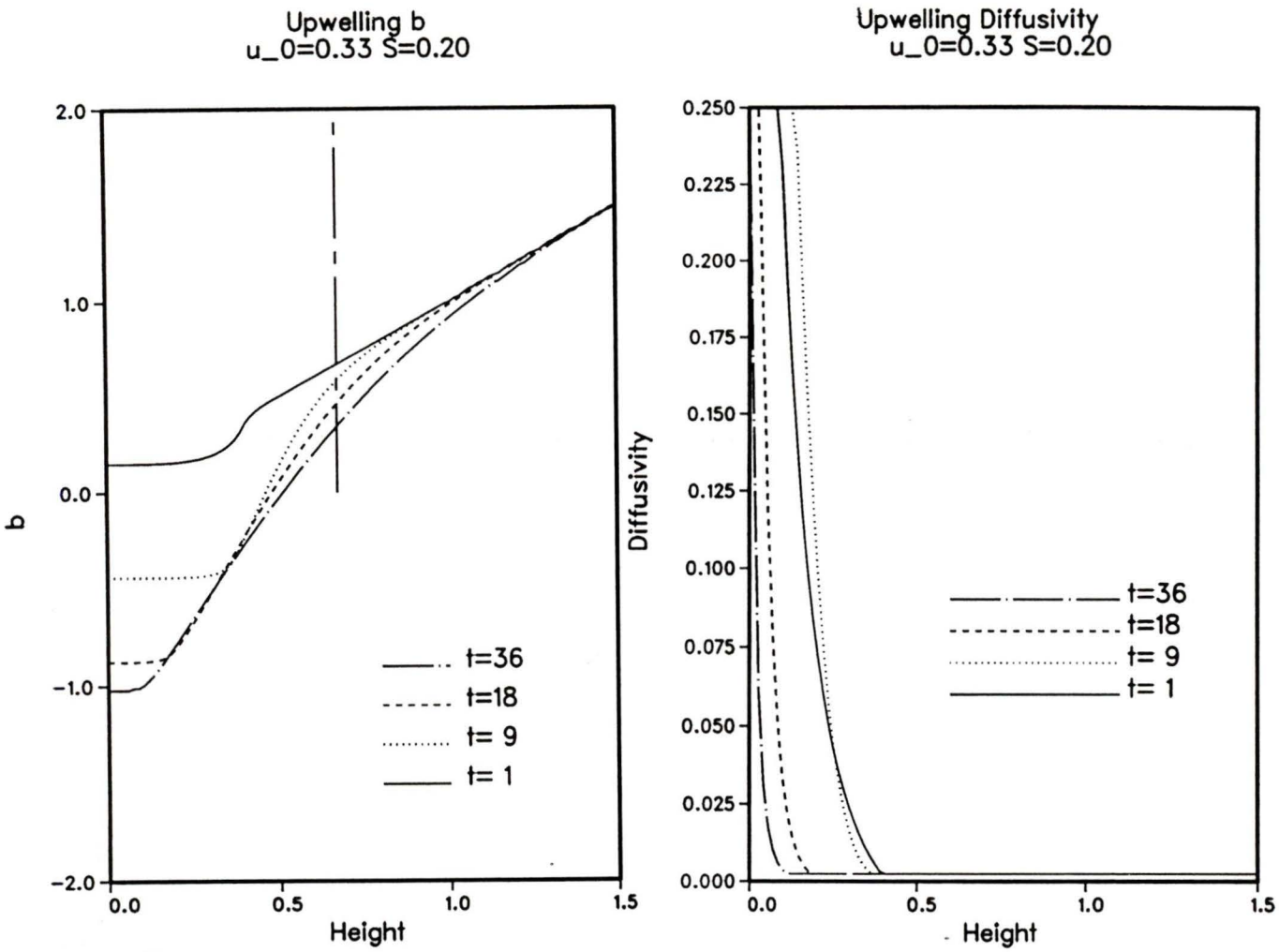

Figure 4.12: Typical time profiles of b and ν' for upwelling favourable flow. The vertical line on the b plot is the Pollard, Rhines and Thompson prediction of initial mixed layer height.

favourable case. As is seen, the Ekman layer does seem to reach an initial height, the theoretical value being indicated by the vertical line on the b plot. The system then seems to show reasonably constant gradients of u and b as the upslope transport is gradually shut down. From $t = 27$ to $t = 36$, the system seems to have reached stationarity except for further growth of the upper boundary (above $z = .7$). The plot of diffusivity shows that the mixing is gradually confined to a smaller and smaller region near the boundary.

Time profiles of $\frac{\partial u}{\partial z}$ and $\frac{\partial b'}{\partial z}$, however, do not fit the expected values, though the mixed layer may still have been growing after $t = 1$. Figure 4.13 shows that

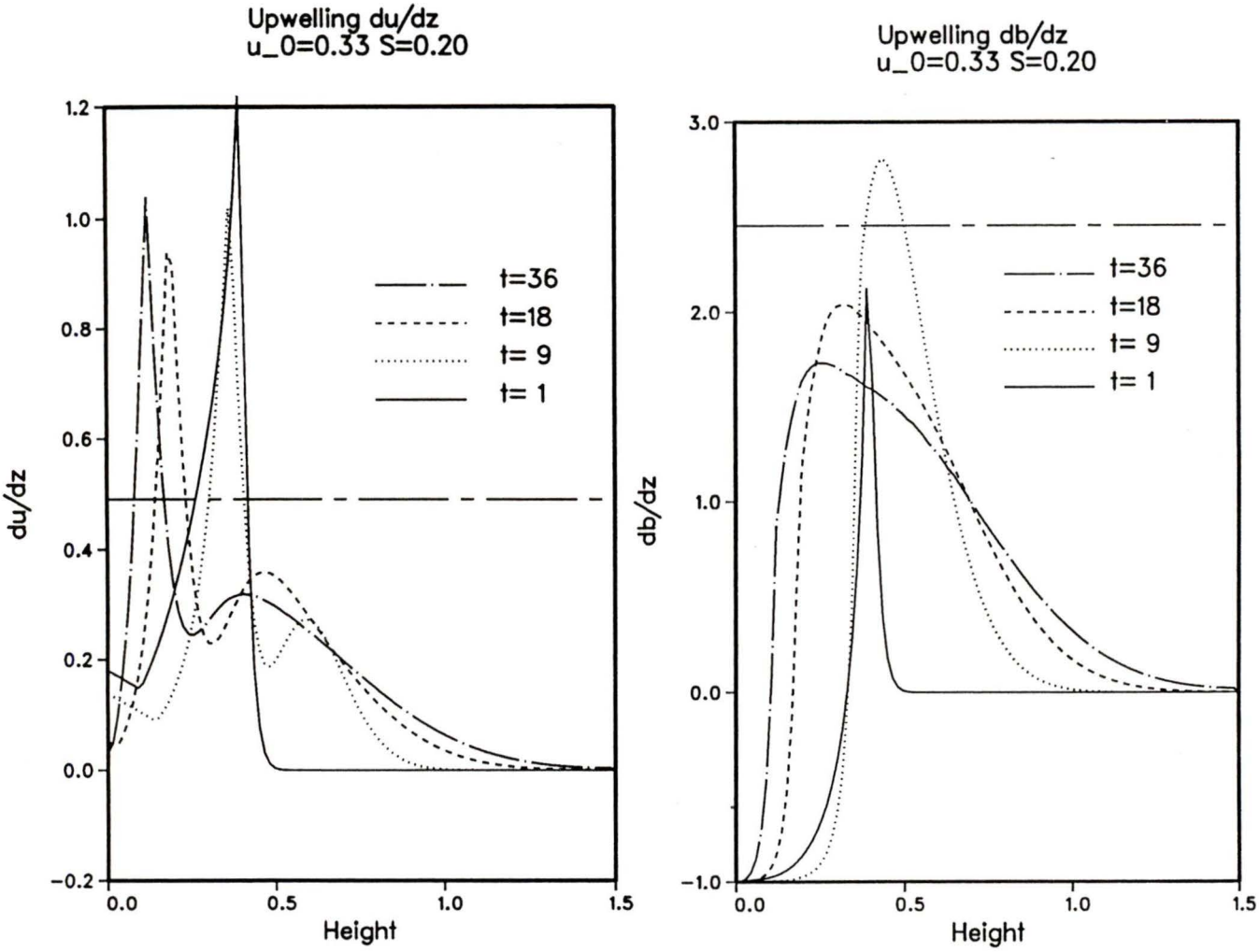

Figure 4.13: Typical profiles of $\frac{\partial u}{\partial z}$ and $\frac{\partial b'}{\partial z}$ for upwelling favourable flow. The horizontal lines are the theoretical prediction of the gradients based on the simple thermal wind balance model.

the gradients are in approximate thermal wind balance, but not at the theoretical values, which are marked by chain-dashed lines. Rather, they are in balance at progressively larger values of h as time progresses.

The tendency for the mixed layer to gradually thicken was analyzed by MR92 and shown to obey a 'slow diffusion' equation. In the downwelling favourable flow case, this diffusion was not a problem since the slow remixing gradually absorbed the slow diffusion. Here, however, the slow diffusion is causing the gradient region above the mixed layer to thicken. A cursory examination of Figure 4.13 shows that u and b are in approximate thermal wind balance, but the balance is at values consistent

with a progressively thicker gradient region.

As with the downwelling favourable flow, runs have been performed at various values of S and D. Table 4.2 shows the run parameters for the 3 cases chosen to compare the numerical results to the simple theory.

Label	S	$\frac{C_d N}{f}$	u_0	h_p	$t_0(f^{-1})$
E	.3	.5	.536	.707	7.9
F	.5	.68	.61	.707	2.5
G	.2	1.	.33	.740	5.5

Table 4.2: Parameters for the Upwelling Cases

Figure 4.14 shows the time series of upwelling transport scaled by initial Ekman flux. It is seen that after the initial layer formation, the transport is consistently greater than the simple model prediction. It is also seen that strong internal wave oscillations are also present after a scaled time of 4. In fact, the system seems to have reached some sort of equilibrium at this point. This equilibrium is also seen in the plots of friction velocity, Figure 4.15.

Again, the model results do not support the simple theory as put forward by GMR. The friction velocity appears linear during the shutdown phase. The equilibrium region again begins after a scaled time of about 4 and is fairly constant. The friction velocity seems independent of the oscillations.

The transport appears to be going into the gradual diffusion of buoyancy into the interior of the flow domain. This assertion is supported by noting that for case 'F', integrating the buoyancy equation 2.4 with respect to z and assuming stationarity, the transport is $\kappa' \cot\theta$. With a Prandtl number of unity, scaling this transport by the initial Ekman flux yields a value of .0025. Comparison of this transport with the end of case 'F' in Figure 4.14 indicates that the average transport is about 5 times this value, so that the system is not in equilibrium.

The tendency for the transport to be larger than that needed to bring the original

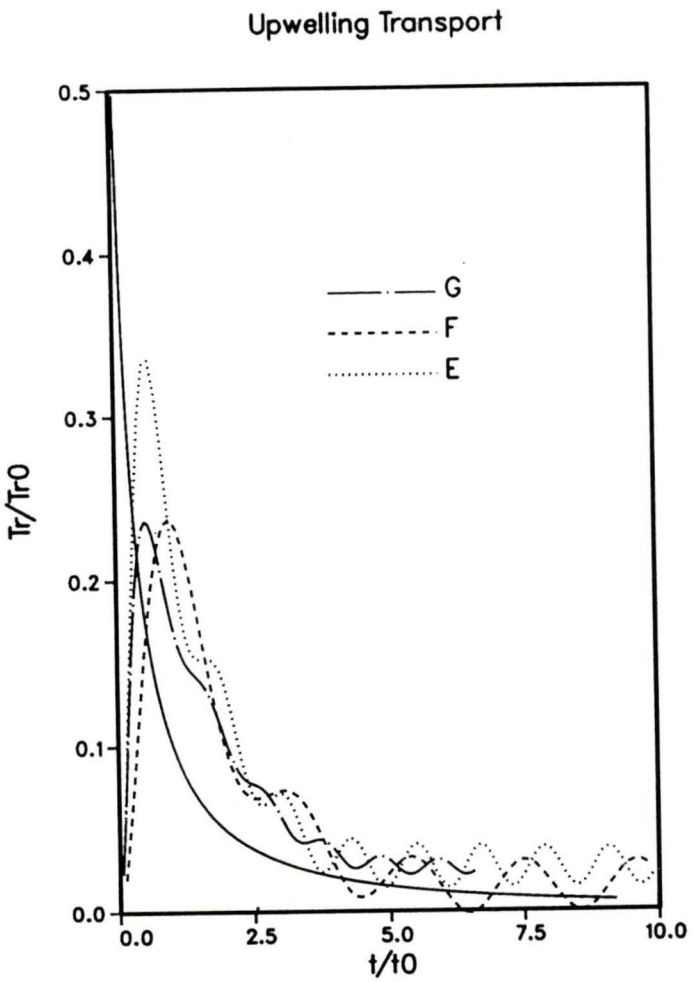

Figure 4.14: Scaled upwelling transport versus scaled time. The solid line is the theoretical prediction.

mixed layer to rest, is also seen in the integrated upwelling transport, Figure 4.16 The scaled integrated transport does not follow the simple model and is above the value of .5 by at least $t/t_0 = 6$. This additionally proves that the assumption of simple advection of an initial mixed height is erroneous. A better theory of the upwelling favourable case is needed, but it appears that the GMR theory may still be of use during the early parts of shutdown until the diffusion processes becomes dominant, or for cases where diffusivity in the far field is much less than in the well-mixed region.

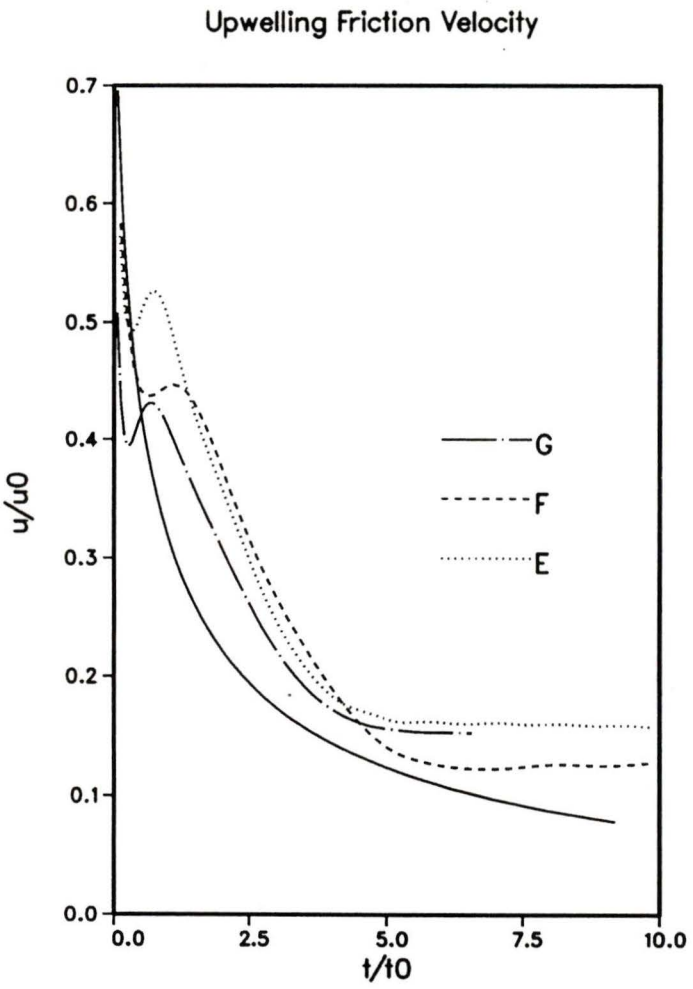

Figure 4.15: Scaled upwelling friction velocities versus scaled time. The solid line is the theoretical prediction.

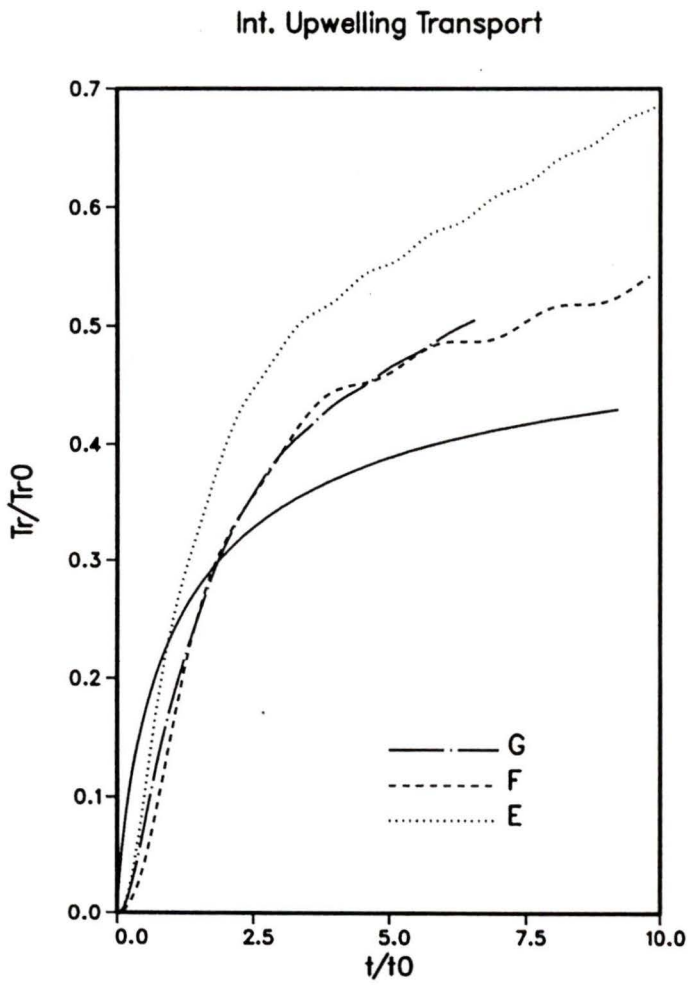

Figure 4.16: Scaled integrated upwelling transport versus scaled time. The solid line is the theoretical prediction.

Chapter 5

Time Dependent Forcing

The results of the previous section are interesting of themselves, but neglect the fact that the interior along slope flow can vary in time. In reality, alongslope flows will be time dependent. Returning to the original motivation for this study, it is appropriate to take as a limiting case a situation where the interior flow is purely sinusoidal in nature. Garrett [17] has determined the amount of net mixing from a complete mixing of the boundary layer, followed by a complete restratification. He concluded that this process is probably not important to net boundary mixing, in the sense that the mixing due to the restratification is weak compared to turbulent mixing rates.

The purpose here is to attempt to directly measure average vertical buoyancy fluxes and residual upslope flow (working against mean background gradient of buoyancy) over a forcing cycle. As shown in Appendix A, the assumption of a variable interior alongslope flow can be implemented in one of two ways.

If it is assumed that the interior alongslope flow is forced by $u_e(t)$, then:

$$F(u_e, u_0) = S(u_e - u_0) + \frac{\partial^2 u_e}{\partial t^2} \tag{5.1}$$

with additional boundary conditions $v_e = \frac{\partial u_e}{\partial t}$ and $b' = u_0 - u_e$.

If it is assumed that the interior flow is in balance with a nondimensionally scaled pressure gradient, then:

$$\frac{\partial u_e}{\partial t} = -\frac{\partial p}{\partial x} \tag{5.2}$$

and $v_e = b'_e = 0$. For both these cases, $u_e = A\cos(\omega t)$ with p chosen to yield the same values of u_e as for the directly forced cases. The new nondimensional parameter which enters the problem is hence ω/f.

For the runs to be presented here, $\omega = 1.44f$. This corresponds to about an $M2$ (twice daily) tidal cycle at a representative mid-latitude. This cycle is too short for shutdown to begin on either part of the forcing cycle, but as described earlier, numerical difficulties prevented a longer period being examined. For these runs, $S = .12, D = 1, \nu'_1 = .25, Pr = 1$ and the amplitude of the forcing was $u_e = 1$.

The runs were chosen so that there were always an exact number of forcing cycles. Two cases, differing only in the far-field conditions described above, were integrated to stationarity as indicated by a time series of boundary velocities, and profiles of u, v, b' and ν' were calculated at 12 equally spaced intervals. Figure 5.1 to 5.4 show profiles of these 4 quantities.

Figure 5.1 shows that there is little difference in the profiles of u for the 2 types of forcing (they are plotted to the same scale). For reference, the downwelling favourable part of the forcing cycle goes from the fourth to the tenth profiles.

As shown in Figure 5.2, the profiles of v, however, reflect the difference in the forcing mechanism. The values of v for the pressure gradient forced cases bear little resemblance to those of the directly forced cases. In fact, when u is near zero (e.g. profiles 4 and 10), the values of v have opposite signs. The penetration of v into the flow interior of the pressure forced case is about half that of the directly forced case. In this case, the two scales of v are also different. The pressure forced case values of v are much smaller than the directly forced case.

Figure 5.3 shows time profiles of buoyancy, with a vertical line plotted for a fully mixed water column. As is seen in Figure 5.3, the boundary conditions influence the profiles (note the bunching of the lines at the top of the directly forced case). In both cases, the depth of the mixed layer is approximately constant, though the directly

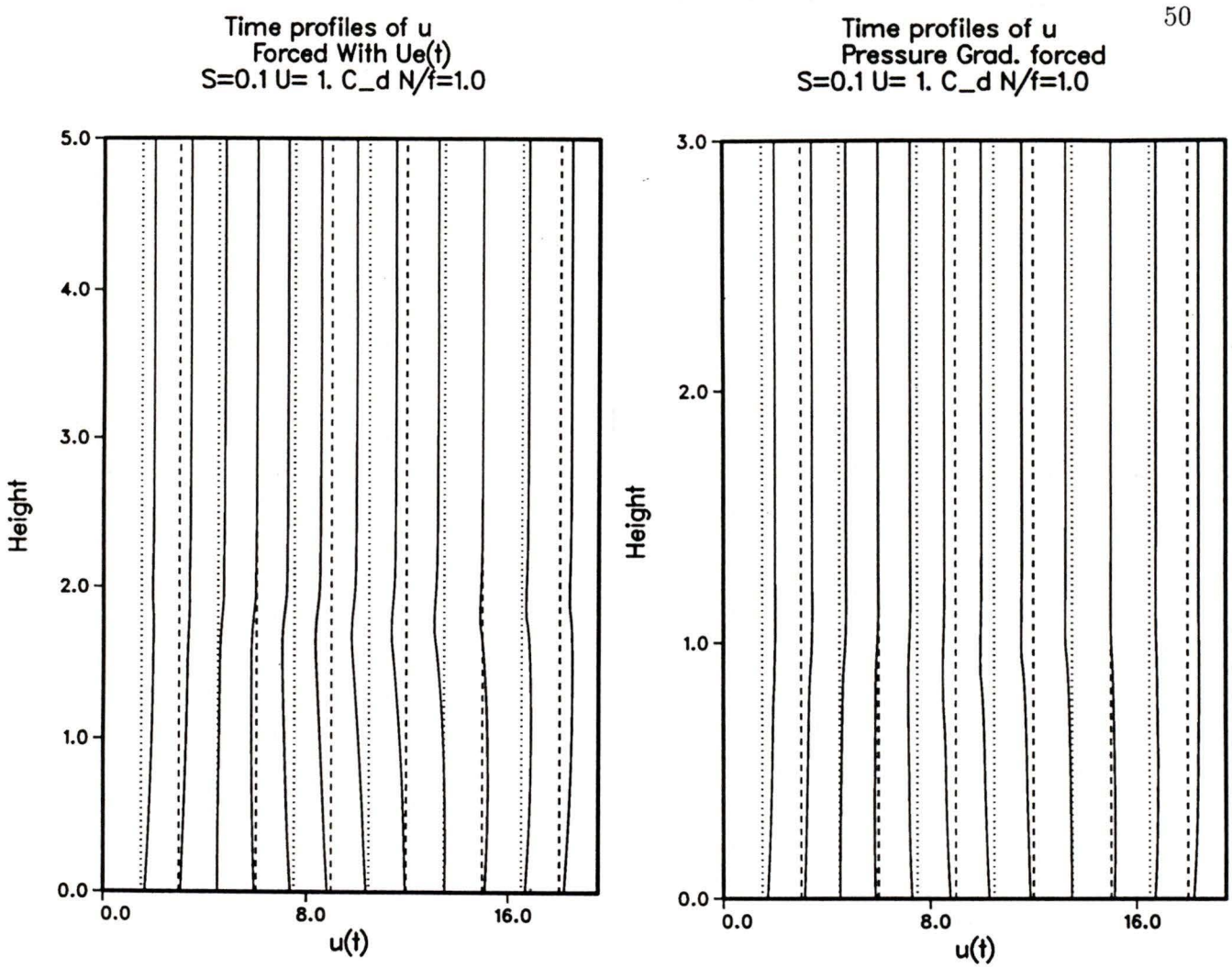

Figure 5.1: Time profiles of u over a forcing cycle for (left) directly forced and (right) forced with a pressure gradient. The vertical dotted and dashed lines are zero reference lines for each profile.

forced case is deeper, and during the downwelling phase appears to restratify to a certain extent.

Figure 5.4 shows profiles of diffusivity ν'. Figure 5.4 shows a radical departure in diffusivity between the two forms of forcing. The directly forced case is less susceptible to the forcing cycle. This is because v is nonzero at the extreme boundary for the directly forced case, and largest when $|u| = 0$. In the pressure gradient forced case, since v is very small, the 'mixing' tends to follow $|u|$ and there is a very large range in $\nu'(z)$.

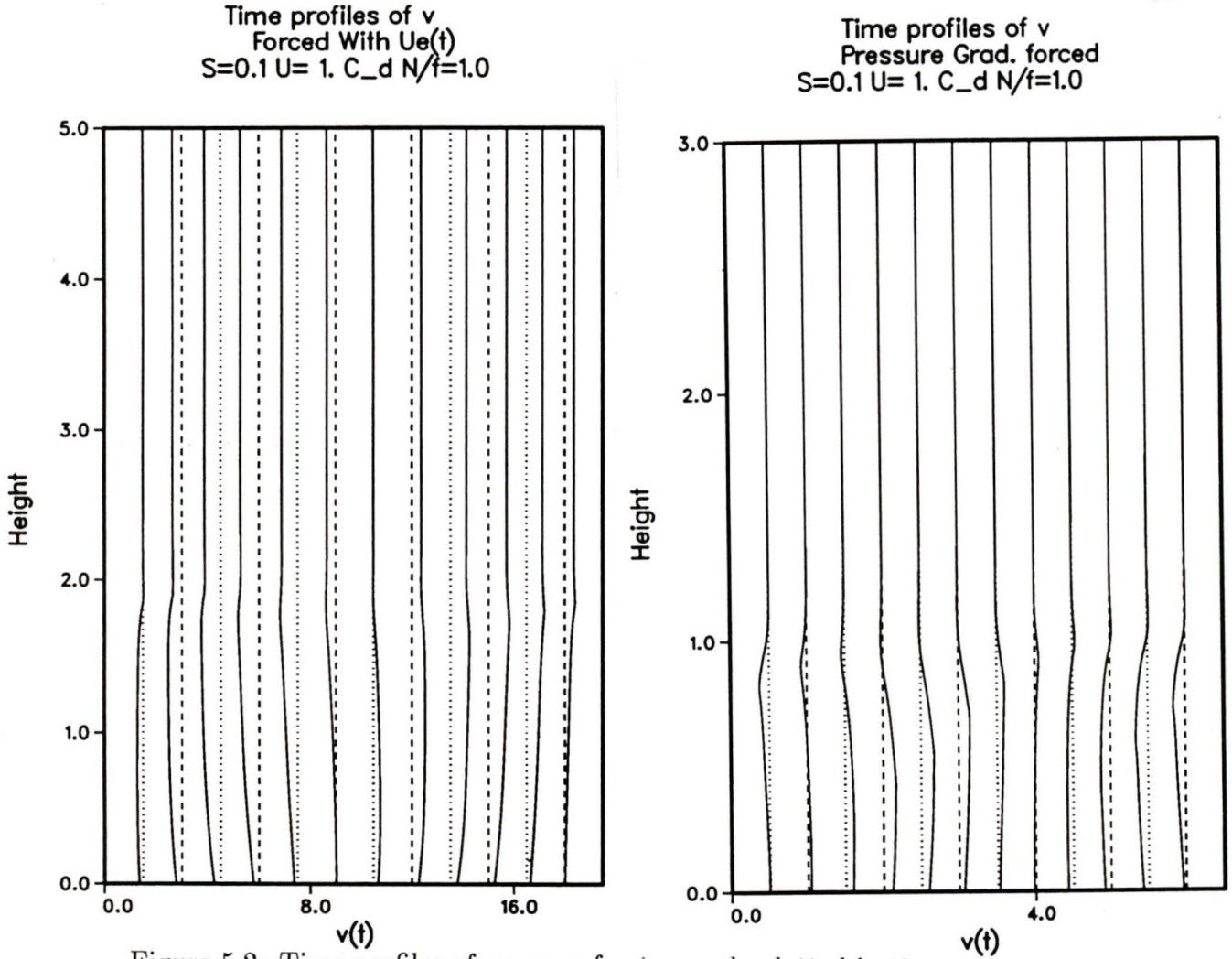

Figure 5.2: Time profiles of v over a forcing cycle plotted in the same manner as u.

5.1 Net Mixing and Parameter Sensitivities

By integrating the numerical models over a few forcing cycles, average vertical buoyancy fluxes $\overline{vb}\sin\theta$ and net upslope movement $\overline{v}$ can be calculated, where the overbars indicate time averages. In order to determine the dependence of these quantities on the parameterization, four runs were considered. The 'base' run will be for a case directly forced, as shown in Figures 5.1 to 5.4. The second case will be identical except that u_e is forced by a pressure gradient. The third case will use a nonunity Prandtl number, and the fourth case will use a different value of the diffusivity near the lower boundary. These cases are summarized in Table 5.1.

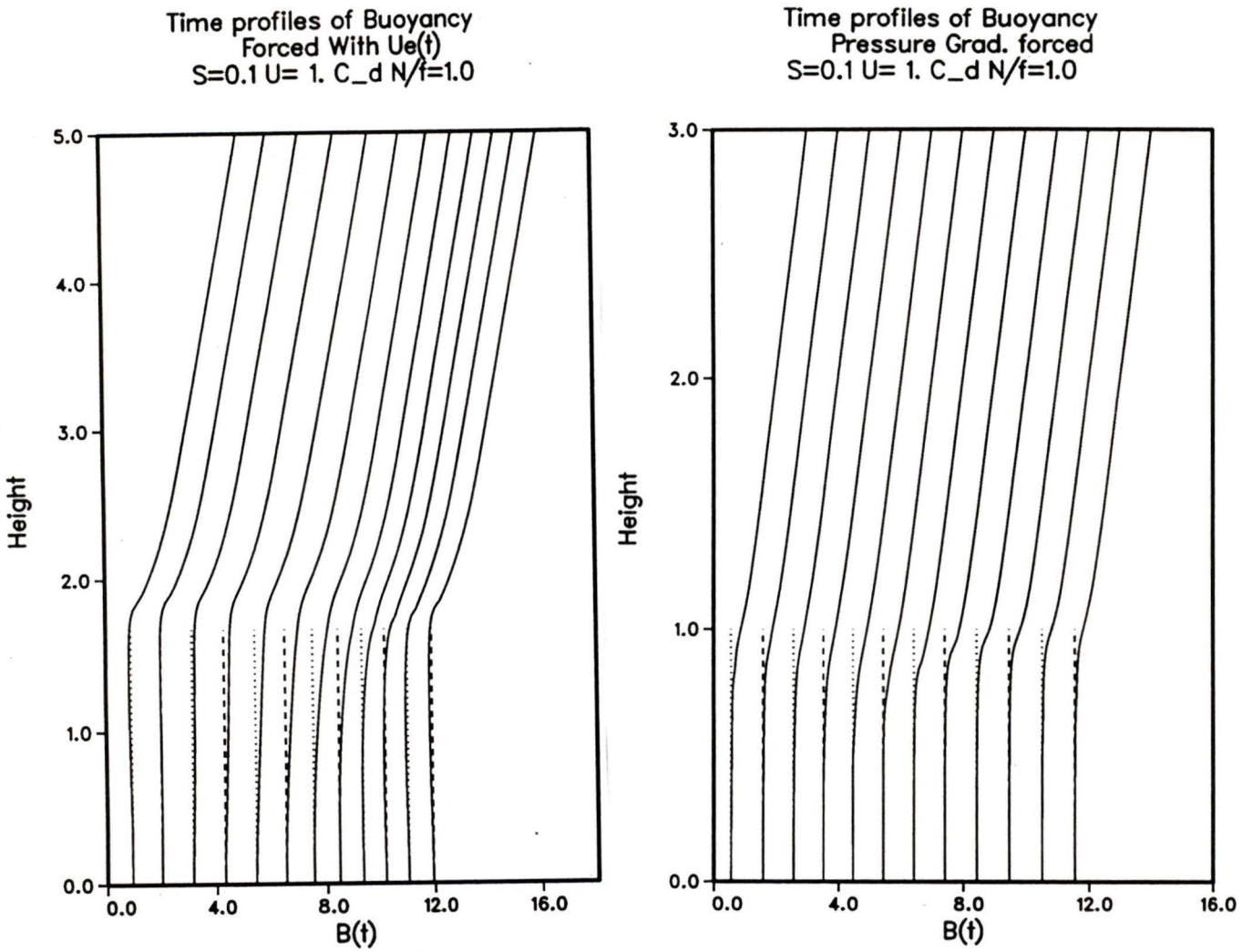

Figure 5.3: Time profiles of b' over a forcing cycle plotted in the same manner as u. The vertical lines are for perfectly mixed water.

Label	Type
H	Base Run
I	Pressure forced
J	$Pr = .8$
K	$\nu_1' = .4$

Table 5.1: Parameters for the Time Dependent Runs

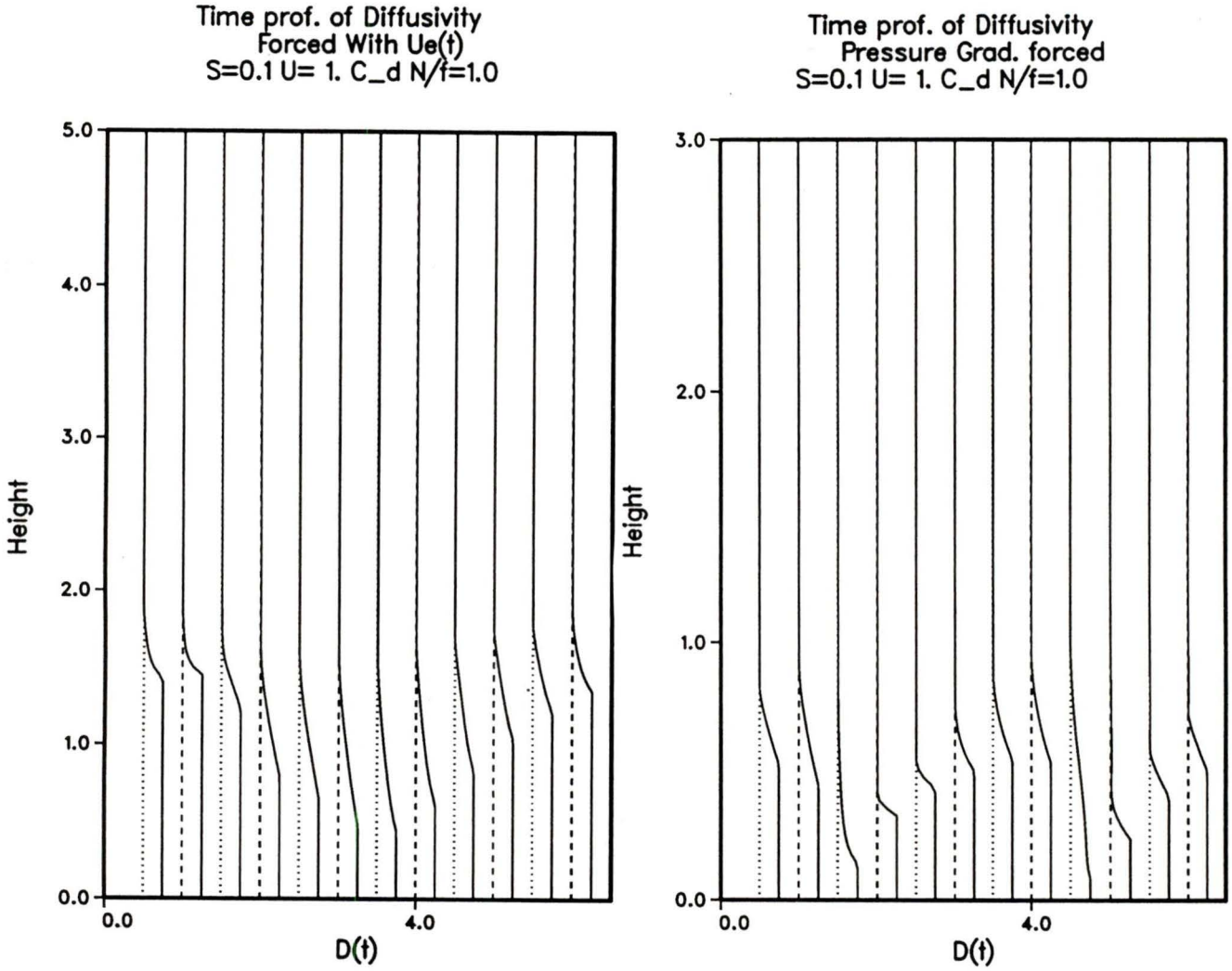

Figure 5.4: Time profiles of ν' over a forcing cycle plotted in the same manner as u.

The values in table 5.1 illustrate a fairly small parameter range, but serve as a starting place for the full parameter sweep which must wait until the resolution of the boundary layer numerical problem. Case 'K' is an obvious choice as it seems plausible that the amount of direct mixing will influence the amount of secondary mixing.

For the Prandtl number test, recent direct numerical simulations of stratified flow (e.g. Ramsden and Holloway, [28]) suggest that nonlinear transfer rates of kinetic and potential energies are very different. These transfer rates can be directly applied to the Reynold's decomposition, resulting in the eddy Prandtl number being low, perhaps even as low as $\frac{1}{2}$. Case 'J' is included to see what effect the Prandtl number might have on net mixing rates.

Figure 5.5 indicates that the net vertical buoyancy flux is not sensitive to the diffusivity or eddy Prandtl number, but is very sensitive to the mode of forcing. Taking the vertical integrals of the time dependent profiles and redimensionalizing yields values of $K_\nu = 3 \cdot 10^{-4} m^2/s$. These values are close to Munk's canonical value. This is the result derived from the deep basin balances discussed in the introduction. Following Armi [13]), scaling the measured values by the relative areas of basins to oceans (order 10^{-4}) will clearly not yield significant average mixing rates for the ocean as a whole and another mechanism must be sought.

These results depend on the parameterization (particularly H), but probably represent the upper limit of K_ν as a strong drag coefficient (D=1) and velocity maximum ($20cm/s$) were used.

The net upslope v, (Figure 5.6) shows less dependence on the form of forcing, but there is still a clear difference. Again, mixing based on net upslope movement is of the same order as the buoyancy flux, and it is concluded that the net movement of water during a mixing cycle will not produce the mixing necessary to balance deep water upwelling. The cases here do not consider topographic irregularities which may in some sense be the ultimate instruments of 'net mixing', however, it is probable that simple flow over boundaries will not provide the buoyancy fluxes or

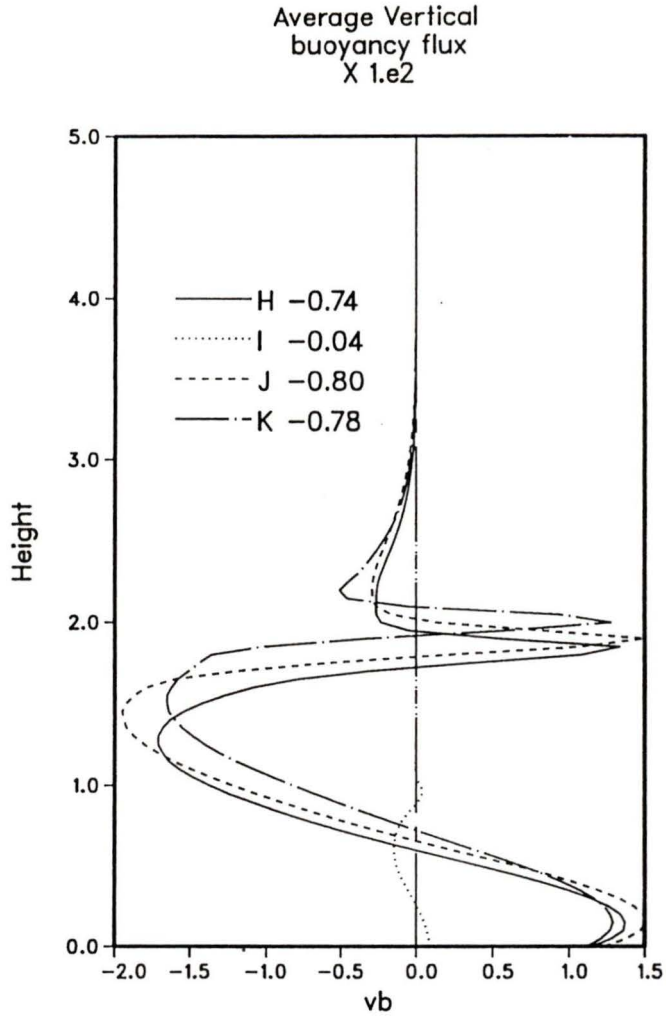

Figure 5.5: Average profiles of vertical buoyancy flux. The numbers are the vertical integrals (X 100).

upslope movement acting against mean gradients.

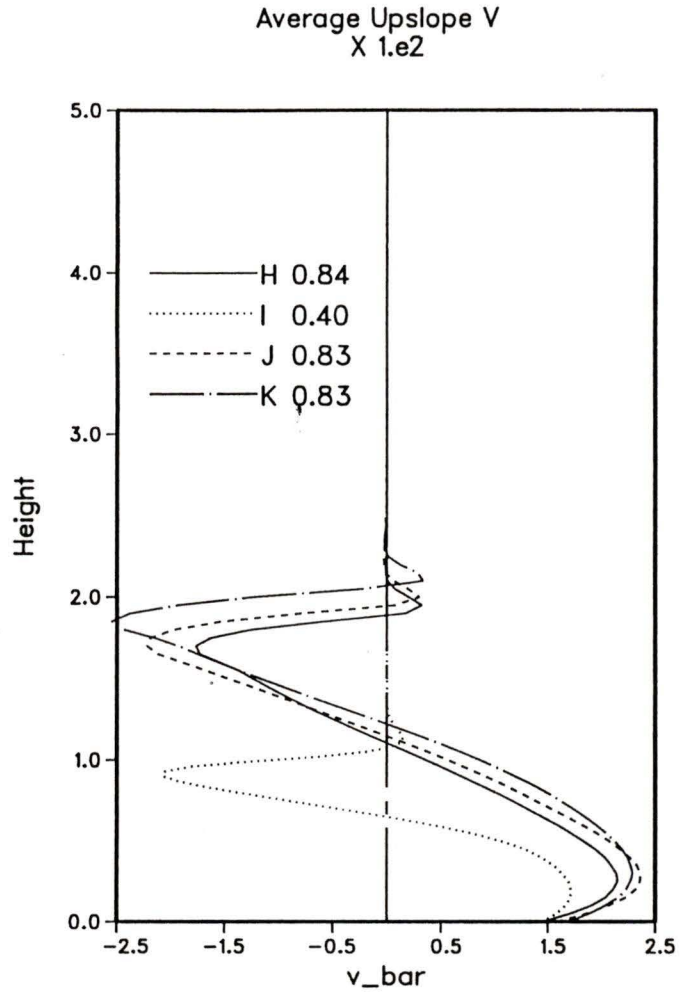

Figure 5.6: Average profiles of upslope velocity. The numbers are the vertical integrals (X 100).

Chapter 6

Conclusions

A series of one dimensional models have been developed to investigate the physics of boundary layers on a sloping bottom in the presence of stable stratification. Several cases have been considered and, in all, the analytic form of eddy viscosity and diffusivity are assumed to be the same.

A numerical model has been confirmed by testing against theoretical predictions of the stationary states of interior stratification and flow, for the case where eddy coefficients of viscosity and diffusivity are constant in time. It is found that the numerical results converge to the theoretical predictions when the mixing extends into the flow interior and the Ekman number is low.

Cases in which diffusivity is restricted to a slab region and the Ekman number is high, are found to converge to a theoretical prediction in regard to the alongslope flow for a range of flow parameters. For the 'ideal' parameterization of a perfectly slab-like behaviour of viscosity and vanishing viscosity in the far field, the prediction of Garrett [17] is confirmed for the alongslope velocity jump at the top of the well mixed layer:

$$U_\infty = -\frac{3}{8} f H \cot\theta \frac{S}{(1+SPr)} \tag{6.1}$$

For non-ideal parameters, the deviation from the theoretical prediction is a complicated function of S and Pr, the values of which define the problem. It is possible,

though, to generate interior flows of opposite sign to the theoretical prediction for quite reasonable parameters, so that the application of the Garrett [17] prediction in nonideal circumstances is tenuous.

Cases in which the interior flow is constant and the eddy viscosities vary as a function of the gradient Richardson number are found to exhibit Ekman layer shutdown for both upwelling and downwelling favourable flow. A simple model is advanced for the downwelling favourable flow based on slow mixing of advected water and thermal wind balance. The model is quite effective in describing the numerical results The natural timescale of shutdown is shown to be $D^{-1}S^{-\frac{3}{2}}f^{-1}$.

A simple model of upwelling favourable flow based on advection of an initial mixed layer is developed, but is not particularly effective in describing the observed behaviour. Diffusion of interior buoyancy from the top of the mixed layer eventually dominates the shutdown process. Before the diffusion process becomes dominant, however, the shutdown process may be described in terms of a mixed layer height which follows a timescale of $D^{-\frac{1}{2}}S^{-1}f^{-1}$.

A model with time-dependent forcing has been developed and driven to stationarity utilizing two different formulations of the boundary conditions. The behaviour of the upslope velocity and interior stratification are quite different when the flow is driven by a prescribed alongslope flow and the upslope flow responds to it than when the interior flow is in balance with a pressure gradient and there is no interior upslope flow.

Direct calculations of buoyancy flux and residual upslope flow integrated over several forcing cycles indicate that average buoyancy flux rates are relatively insensitive to the parameterization, but very sensitive to the form of the boundary conditions. In any event, the secondary mixing from tidal (or other) cycles is probably weak in the sense that the secondary average buoyancy fluxes and upslope transports do not generate large (compared to primary mixing rates) boundary mixing.

6.1 Improvements

The outstanding problem which needs to be addressed is the need to better represent the log layer and prevent the numerical instabilities when velocities are weak near the boundary. Several ideas come to mind, but the most logical is to employ a multigrid technique in which the log layer is represented directly in logarithmic coordinates. At present, only the top of the log layer is modelled, but with the inclusion of the logarithmic coordinates, velocities and viscosities could be zero at the boundary and vary smoothly to the top of the constant stress (Holton [29]) log layer.

MR92 and others also show that the dynamics of long-propagating deep boundary currents are usually associated with tilted isopycnals which will contain a significant amount of potential energy. A proper treatment of the Ekman layer problem should probably include a provision for tilted isopycnals in thermal wind balance with alongslope velocity. The theory and code have been evaluated for this case and are ready to use.

Of course, there are many other improvements which could be made to the numerical models, but until the log layer problem is solved, they are insignificant by comparison.

Bibliography

[1] A. Mantyla and J. Reid, Abyssal characteristics of the World Ocean waters, *Deep-Sea Res.*, Vol 30, No. 8A, 805-833, 1983.

[2] P. MacCready and P. Rhines, Slippery bottom boundary layers on a slope. *J. Phys. Oceanogr.* (in press), 1993.

[3] L. Armi and R. Millard, The bottom boundary layer of the deep ocean, *J. Geophys Res.*, **81**, 4983-90, 1976.

[4] S. Thorpe, P. Hall and P. Martin, The variability of mixing on the continental slope, *Phil. Trans. R. Soc. London*, **A331**, 183-194, 1990.

[5] W. Munk, Abyssal recipes, *Deep-Sea Res.* **13**, 207-30, 1966.

[6] M. Gregg, Diapycnal mixing in the thermocline: A review, *J. Geophys. Res.*, **92**, 5249-86, 1987.

[7] H. Yamazaki and R. Lueck, Why oceanic dissipation rates are not lognormal, *J. Phys. Ocean.*, **20**, No. 12, 1907-18, 1990.

[8] N. Hogg, P. Biscayne, W. Gardner and W. Schmitz Jr., On the transport and modification of Antarctic Bottom Water in the Vema Channel, *J. Mar. Res.*, **40** (suppl.), 231-263, 1982.

[9] A. E. Gargett, Vertical eddy diffusivity in the ocean interior, *J. Mar. Res.*, **42**, 359-393, 1984.

[10] C. Garrett, Mixing in the ocean interior, *Dyn. Atmos. Oceans*, **3**, 239-65, 1979.

[11] F. Bryan, Parameter sensitivity of primitive equation ocean general circulation models, *J. Phys. Oceanogr.*, **17**, 970-985, 1979.

[12] P. Cummins, G. Holloway and A. Gargett, Sensitivity of the GFDL model to parameterization of vertical diffusivity, *J. Phys. Oceanogr.*, **20**, 817-830, 1990.

[13] L. Armi, Some evidence for boundary mixing in the deep ocean, *J. Geophys. Res.* **83**, 1971-1979, 1978.

[14] O. Phillips, J. Shyu and H. Salmun, An experiment on boundary mixing: mean circulation and transport rates, *J. Fluid Mech.*, **173**, 473-499, 1986

[15] S. Thorpe, Current and temperature variations on the continental slope, *Phil. Trans. R. Soc. London*, **A323**: 471-517, 1987.

[16] C. Garrett, The role of secondary circulation in boundary mixing, *J. Geophys. Res.*, **95**, 989-93, 1990.

[17] C. Garrett, Marginal mixing theories, *Atmos. Ocean* , **29**, 313-39, 1991.

[18] J. Trowbridge, and S. Lentz, Asymmetric behaviour of an oceanic boundary layer above a sloping bottom, *J. Phys. Oceanogr.*, **21**, 1171-85, 1991.

[19] C. Garrett, P. MacCready and P. Rhines, Boundary mixing and arrested Ekman layers: Rotating stratified flow near a sloping boundary, *Ann. Rev. Fluid Mech.*, **25**:, 291-323, 1993.

[20] P. MacCready, Frictional slowing of rotating stratified flow over a sloping boundary, Ph.D. thesis, Univ. of Wash, 1991.

[21] P. Roache, Computational Fluid Dynamics, *Hermosa Publishers*, ISBN 0-913478-0509, 1972.

[22] W. Press, B. Flannery, S. Teukolsky and W. Vetterling, Numerical Recipes, *Cambridge Univ. Press*, 1987.

[23] Parker MacCready, Personal Communication, September 16, 1992.

[24] L. Howard, A note on a paper of J. W. Miles, *J. Fluid Mech.*, **10**, 509-512, 1961.

[25] G. Weatherly and P. Martin, On the structure and dynamics of the oceanic bottom boundary layer, *J. Phys. Oceanogr.*, **8**, 557-570, 1978.

[26] R. Pollard, P. Rhines and R. Thompson, The deepening of the wind-mixed layer, *Geophys. Fluid Dyn.*, **3**, 381-404, 1973.

[27] R. Thompson, Stratified Ekman boundary layers, *Geophys. Fluid Dyn.*,**5**, 201-10, 1973.

[28] D. Ramsden and G. Holloway, Energy transfers across an internal wave-vortical mode spectrum, *J. Geophys. Res.*, **97**, No. C3, 3659-3683, 1992.

[29] J. Holton, An Introduction to Dynamic Meteorology, *Academic Press*, ISBN 0-12-354360-6, 1979.

Appendix A

Development of the Nondimensional Equations

For reference, equations 2.1 to 2.4 are repeated here and serve as the starting point for the nondimensionalization.

$$\frac{\partial U}{\partial T} - fV = -\frac{1}{\rho_0}\frac{\partial \overline{P}}{\partial X} + \frac{\partial}{\partial Z}\left(\nu\frac{\partial U}{\partial Z}\right) \tag{A.1}$$

$$\frac{\partial V}{\partial T} + fU = -\frac{1}{\rho_0}\frac{\partial \overline{P}}{\partial Y} + B\sin\theta + \frac{\partial}{\partial Z}\left(\nu\frac{\partial V}{\partial Z}\right) \tag{A.2}$$

$$0 = -\frac{1}{\rho_0}\frac{\partial \overline{P}}{\partial Z} + B\cos\theta - \frac{\partial}{\partial Z}(\overline{W^2}) \tag{A.3}$$

$$\frac{\partial B}{\partial T} + VN^2\sin\theta = \frac{\partial}{\partial Z}\left(\kappa\frac{\partial B}{\partial Z}\right) \tag{A.4}$$

Taking the Y derivative of Equation A.3, rearranging the pressure term and integrating with respect to Z:

$$-\frac{1}{\rho_0}\frac{\partial \overline{P}}{\partial Y} = -N^2 Z\sin\theta\cos\theta + G(Y,T) \tag{A.5}$$

with $G(Y,t)$ to be evaluated. Putting A.5 into equation A.2:

$$\frac{\partial V}{\partial T} + fU = G(Y,T) - N^2 Z\sin\theta\cos\theta + B\sin\theta + \frac{\partial}{\partial Z}\left(\nu\frac{\partial V}{\partial Z}\right) \tag{A.6}$$

In order to evaluate $G(Y,T)$, the defining equations A.1, A.4 and A.6 are evaluated sufficiently far from the boundary such that diffusive terms are deemed to vanish and $U = U_e(T)$. If this assumption is employed, one obtains:

$$\frac{\partial U_e}{\partial T} = fV_e + \frac{\partial \overline{P}}{\partial X} \tag{A.7}$$

$$\frac{\partial V_e}{\partial T} + fU_e = G(Y,T) - N^2 Z \sin\theta\cos\theta + B\sin\theta \tag{A.8}$$

$$\frac{\partial B}{\partial T}v + fV_e N^2 \sin\theta = 0 \tag{A.9}$$

At this point, a choice must be made as to whether U_e is in balance with the pressure gradient, or no pressure gradient exists and U_e is in balance with V_e (and B). If the first choice is made, then $V_e = 0, B_e = 0$ and:

$$G(Y,T) = fU_e + N^2 Z_e \sin\theta\cos\theta \tag{A.10}$$

Choosing $B' = B + N^2(Z - Z_e)\cos\theta$, and after nondimensionalizing (see below), one obtains equation 2.9 and

$$\frac{\partial V}{\partial T} + f(U - U_e) = B'\sin\theta + \frac{\partial}{\partial Z}\left(\nu\frac{\partial V}{\partial Z}\right) \tag{A.11}$$

Hence, for this case, $F(u_e, u_0) = 0$. Equation A.11 is nondimensionalized in the same manner as demonstrated below. If the second choice (no pressure gradient) is made, equation A.7 is put into equation A.9 to obtain:

$$\frac{\partial B_e}{\partial T} = -N^2 f^{-1}\sin\theta\frac{\partial U_e}{\partial T} \tag{A.12}$$

combined with

$$\frac{\partial B}{\partial Y} = N^2\sin\theta \tag{A.13}$$

and

$$\frac{\partial B}{\partial Z} = N^2\cos\theta \tag{A.14}$$

in this region, this yields:

$$B_e = N^2\sin\theta f^{-1}U_e + YN^2\sin\theta + ZN^2\cos\theta + C \tag{A.15}$$

which implies:

$$G(Y,T) = -YN^2 \sin\theta - C\sin\theta + f(1+S)U_e + f^{-1}\frac{\partial^2 U_e}{\partial T^2} \qquad \text{(A.16)}$$

where $S = N^2 \sin^2\theta / f^2$. Putting A.16 into A.6:

$$\frac{\partial V_e}{\partial T} + fU = (B - ZN^2\cos\theta - YN^2\sin\theta)\sin\theta - C\sin\theta f(1+S)U_e + f^{-1}\frac{\partial^2 U_e}{\partial T^2} + \frac{\partial}{\partial Z}\left(\nu\frac{\partial V}{\partial Z}\right) \qquad \text{(A.17)}$$

$B' = B - ZN^2\cos\theta - YN^2\sin\theta$. C is evaluated at $T = 0$ when $B' = 0$, $U_e = U_0$ and $\frac{\partial^2 U_e}{\partial T^2} = 0$, which yields $C = fSU_0/\sin\theta$.

Finally,

$$\frac{\partial V_e}{\partial T} + f(U - U_e) = B'\sin\theta + fS(U_e - U_0) + f^{-1}\frac{\partial^2 U_e}{\partial T^2} + \frac{\partial}{\partial Z}\left(\nu\frac{\partial V}{\partial Z}\right) \qquad \text{(A.18)}$$

Velocities are nondimensionalized with $U = fH\cot\theta u$ and buoyancy with $B' = N^2 H\cos\theta b'$ and with length and time scales given in the body to yield equations 2.7 to 2.9. For this case,

$$F(u_e, u_0) = S(u_e - u_0) + \frac{\partial^2 u_e}{\partial t^2} \qquad \text{(A.19)}$$

Note that in all cases, $\cos\theta$ is taken to be ≈ 1 as a necessity to simplify the equations of motion, as large angles would need to include the other components of f in the equations of motion.

Appendix B

Programming and Archival Considerations

All the numerical models were developed on the IRIS computer at UVIC under account "dave@aquarius.seaoar.UVic.CA" (Internet number 128.189.71.2). The results have been removed, but the Fortran programs have been retained. Some additional simulations were performed on faster machines which do not affect the archival process. The relevant files are contained in the dave/models directory in the following subdirectories.

1. low_ekman_old: The low Ekman number programs
2. crank: The high Ekman number programs
3. test_terms: Programs to determine the stationarity of endstates.
4. mcr_expl: The Ekman layer shutdown programs
5. time_dep: Time dependent forcing programs (Direct forcing of u_e).
6. pressure: Time dependent forcing programs where u_e is in balance with a pressure gradient.

In addition, various programs to manipulate data are contained in dave/utilities. These programs prepared data for plotting which was executed under DISSPLA on

the IOS VAX system under account and directory [DRCEOS.THESIS_PLOTS] (Internet number 134.87.12.1). This thesis was prepared with LaTeXon VAX phasta.uvphys.UVic.CA (Internet number 128.189.67.1) under account, directory and file [RAMSDEN.THESIS]BODY.TEX. All these files will be retained for 6 months from publication date whence they will exist on backup tapes only (but available on request).

A sample program, taken from the Ekman shutdown series follows:

```
c*********************************************
c
c               CEOS : CEOR
c                University of Victoria
c                Victoria, BC V8W3P2
C
C*********************************************
c
c        module name: dave/models/mcr_expl/program.f
c
c        programmer's name: Dave Ramsden
c
c        date of writing: may 29 1992
c
c        date(s) of modification:
c
c        jun 09 1992:        add du/dz b.c.                  (version 2.0)
c        jun 22 1992:        add layer mixed layer depth     (version 2.1)
c        jul 17 1992:        add snapshots of U,V,B',diff    (version 2.2)
c        jul 27 1992:        remove time series except for u*(version 2.3)
c        jul 27 1992:        use nondimensional diffusivity  (version 2.4)
c        jul 28 1992:        introduce some initial shear    (version 2.5)
c        sep 11 1992:        add nu_max rather than just .25 (version 2.6)
c
c*****************************************************************
c
c        method:  uses MacCready and Rhines type dissipation with
c                 a log layer boundary condition
c
c*****************************************************************
c
       program mcr_explicit
c
       implicit none
c
       real version/2.6/
```

```
      character*24 fdate        ! Unix date stamp function
c
      integer nz
c
c      nz                total number of grid points in z direction
c
      parameter (nz=1001)
c
      real*8 bprime(nz),u(nz),v(nz),u_0,u_e
c
c      bprime      deviation of buoyancy from background value
c      u           alongslope velocity
c      v           upslope velocity
c      u_0         far field value of alongslope velocity at t=0.
c      u_e         far field alongslope vel. as fn of time
c
      real*8 prandtl,zmax,dz,dzinv2,dzsqin,z,N_over_f,C_d,nu_max
c
c      prandtl     Prandtl number nu/kappa
c      zmax        last point in domain
c      dz          zmax/(nz-1)
c      dzinv2      1./(2.*dz)
c      dzsqin      1./dz**2
c      z           current value of height (0-zmax)
c      N_over_f    N/f
c      C_d         drag coefficient
c      nu_max      maximum value of nu in the mixing region
c
      real*8 tstart,tmax,dt,dt2,dtfac,dt_diag,v_int,time
c
c      tstart      start time in 1/f units
c      tmax        end time in 1/f units
c      dt          time step interval
c      dt2         dt/2.
c      dtfac       1/(1+dt**2/4) factor used in implicit time step
c      dt_diag     diagnostic interval
c      v_int       integral of v [0-1]
c      time        the current time
c
      integer j,k,interval,nt,nsteps,ntsnap
c
c      j,k         dummy indices
c      interval    time series interval
c      nt          step number
c      nsteps      total number of steps (=tmax/dt)
c      ntsnap      snapshot interval
c
```

```
      real*8 S,bgrad,v_layer
c
c       S           The Burger number
c       bgrad       scaling for boundary gradient  Cd/(nu*sin(theta))
c                   sin(theta)=sqrt(S)*f/N
c          ---->    bgrad=C_d*N/f/(sqrt(S)*nu)
c       vlayer      velocity at bottom of Ekman layer (bottom of model)
c
      real*8 rhs(nz,3),dfdz(nz),diff(nz)
c
c       rhs         right hand sides of equations
c       diff        diffusivity (z)
c       dfdz        d(diff(z))/dz
c
      real*8 work1(nz),work2(nz)
c
c       work1,work2 workspaces needed for crank-nicholson
c       bkn         workspace  needed for crank-nicholson
c
      real*8 modsave,rich(10),shear(10)
c
      real etime,time1,utime,systime,tempval
c
c       etime       standard unix timing routine
c       time1       dummy function target location
c       utime       user time (minutes)
c       systime     system time (minutes)
c       tempval     temporary storage
c
      real*4 tser(100),transport(100)
      1,        l_depth(100)              ! time series
c
c*****************************************************************
c
      common /params/S,tmax,zmax,u_0,tstart,dt_diag,prandtl
      1, N_over_f,C_d,nu_max
c
c*****************************************************************
c
      tstart=0.d0
c
      call getpars
c
      write(9,2000)version,fdate()
 2000      format(' Boundary Layer (Mcr-Rhi): Version',f5.1,2x,a24)
c
c       set up some defaults, solve for the arrays needed for Cr-Nich
```

```
c
      dz=zmax/dfloat(nz-1)
      dzinv2=.5d0/dz
      dzsqin=1.d0/dz**2
      u_e=u_0
c
      dt=.25*dz**2/nu_max                !1/4*dz**2/diff(max)
      dt2=dt/2.d0
      dtfac=1.d0/(1.d0+(dt**2)/4.d0)
      nsteps=ifix((tmax-tstart)/dt+.5)
c
      interval=nsteps/100
      if(interval.eq.0)interval=1
c
      tempval=dt
      if(tmax.lt.47.d0)then
        ntsnap=ifix(.5/dt)
      else
        ntsnap=ifix(10./dt)
      endif
c
c      bgrad=2.d-3*35.d0/(.01*dsqrt(S))        !N/f=35, Cd=.002 nu=.01
c
      bgrad=C_d*N_over_f/(nu_max*dsqrt(S))
      bgrad=bgrad*20.d0                       ! this should be REMOVED
c                                             ! eventually for TRUE N/f
c      start option if new fields
c
      if(tstart.eq.0.)then
c
        do j=2,nz
          u(j)=u_0
          v(j)=0.d0
          bprime(j)=0.d0
        enddo
c
c      introduce some initial shear to get program going
c
c         do j=2,50
c           u(j)=u_0*(.5+float(j)/50.)
c         enddo
c
c      set conditions at boundary
c
        u(1)=u(2)-dz*bgrad*u(2)*abs(u(2))
        v(1)=0.d0
        bprime(1)=dz
```

```
c
      else
c
        read(11)u,v,bprime,diff
        close(unit=11)
      endif
c
      if(nsteps/ntsnap.gt.20)stop 'too many snapshots'
c
      do nt=1,nsteps
c
c      if(mod(nt,100).eq.1)then
c          write(*,*)'at time', time
c          do j=1,10
c             write(*,*)u(j),v(j),bprime(j)
c          enddo
c      endif
c
c      solve for diffusivity and df/dz based on a richardson number
c      criterion        db/dz/(du/dz^2+dv/dz^2)^.5
c      split the do loops to enhance vectorization
c      and use centered differences except upwind value for first point
c
      work1(1)=0.
      work2(1)=0.
      work1(2)=(u(2)**2+v(2)**2)/dz**2
      work2(2)=0.                          ! db/dz=0 in BBL
c
      do j=3,nz-1
          work1(j)=((u(j+1)-u(j-1))**2+(v(j+1)-v(j-1))**2)/(4.*dz**2)
          work2(j)=(bprime(j+1)-bprime(j-1))/(2.*dz)+1.
      enddo
c
      work1(nz)=1.d-10
      work2(nz)=1.        ! make sure diffusivity low at z=zmax
c
      do j=2,nz-1
          work1(j)=dmax1(work1(j),1.d-10)
      enddo
c
c      do j=1,10
c         shear(j)=work1(j)
c      enddo
c
      work2(1)=.25d0
c
      do j=2,nz
```

```
            work1(j)=s*work2(j)/work1(j)
            diff(j)=nu_max
          enddo
c
c          do j=1,10
c              rich(j)=work1(j)
c          enddo
c
c          set ramp function for diffusivity
c
          do j=2,nz
            if(work1(j).gt..2d0)then
              if(work1(j).gt..3d0)then
                diff(j)=.0025d0
              else
                diff(j)=nu_max-(work1(j)-0.2d0)*(nu_max-.0025d0)/.1d0
              endif
            endif
          enddo
c
          diff(1)=nu_max
          diff(nz)=.25d-2
c
c          get d(diff)/dz
c
          do j=2,nz-1
            dfdz(j)=(diff(j+1)-diff(j-1))/(2.d0*dz)
          enddo
c
c          form rhs of 3 equations (1,2,3) --> (u,v,b):
c
           do j=2,nz-1
c
c          time step the equations
c          this is ftcs (Forward Time, Centered Space) on dfdz term
c
            rhs(j,1)=dfdz(j)*(u(j+1)-u(j-1))*dzinv2
         1 +diff(j)*(u(j+1)+u(j-1)-2.d0*u(j))*dzsqin
c
            rhs(j,2)=s*bprime(j)+u_e+dfdz(j)*(v(j+1)-v(j-1))*dzinv2
         1 +diff(j)*(v(j+1)+v(j-1)-2.d0*v(j))*dzsqin
c
            rhs(j,3)=dfdz(j)/prandtl*(bprime(j+1)-bprime(j-1))*dzinv2
         1   +diff(j)/prandtl*(bprime(j+1)+bprime(j-1)-2.d0*bprime(j))
         1   *dzsqin+dfdz(j)-v(j)
c
           enddo
```

```
c
c       time step the equations, treating the coriolis term implicitly
c
C          do j=2,10
c            write(9,112)j,(rhs(j,k),k=1,3)
c          enddo
c
           do j=2,nz-1
c
             rhs(j,1)=u(j)+rhs(j,1)*dt+v(j)*dt2
             rhs(j,2)=v(j)+rhs(j,2)*dt-u(j)*dt2
c
           enddo
c
c       split the do loop to enhance vectorization
c
           do j=2,nz-1
c
             u(j)=(rhs(j,1)+rhs(j,2)*dt2)*dtfac
             v(j)=(rhs(j,2)-rhs(j,1)*dt2)*dtfac
c
             bprime(j)=bprime(j)+rhs(j,3)*dt
c
           enddo
c
c       update boundary conditions (implement log layer)
c
           bprime(1)=bprime(2)+dz
           v_layer=dsqrt(v(2)**2+u(2)**2)
c
           u(1)=u(2)-dz*bgrad*v_layer*u(2)
           v(1)=v(2)-dz*bgrad*v_layer*v(2)
c
c          write(9,*)'step ',nt
c          do j=1,10
c            write(9,112)j,u(j),v(j),bprime(j),diff(j),shear(j),rich(j)
c112            format(1x,i4,2x,6(d10.3,2x))
c          enddo
c
c          if(nt.eq.20)stop
c
           time=tstart+dfloat(nt)*dt
c
           if(mod(nt,interval).eq.0)then
c
              k=nt/interval
              tser(k)=u(1)
```

```
c
c         integrate (0-zmax) V
c
              v_int=v(1)/2.
              do j=2,nz-1
                v_int=v_int+v(j)
              enddo
c
              v_int=v_int*dz
c
              transport(k)=v_int
c
              l_depth(k)=0.d0
c
c         get mixed layer height based on diffusivity profile
c
              do j=nz,1,-1
                 if(diff(j).gt..249d0)then
                   l_depth(k)=dz*dfloat(j-1)
                   go to 3000
                 endif
              enddo
c
3000           continue
c
           endif
c
           modsave=dmod(time,dt_diag)
           if(modsave.lt.dt/2.d0.or.nt.eq.nsteps)then
c
            write(9,*)'at time',tstart+float(nt)*dt
            write(9,*)' '
            write(9,*)' profiles of u,v,bprime,diff,dfdz'
c
            write(9,*)' '
            do j=1,nz,10
               z=float(j-1)*dz
               write(9,9)z,u(j),v(j),bprime(j),diff(j),dfdz(j)
9               format(1x,d11.3,1x,5d11.4)
            enddo
c
           endif
c
c         check for things going wonky
c
           if(dmod(time,1.d0).lt.dt/2.d0)then
              do j=1,nz
```

```
                if(dabs(u(j)).gt.10.d0)go to 1000
                if(dabs(v(j)).gt.10.d0)go to 1000
                if(dabs(bprime(j)).gt.10.d0)go to 1000
              enddo
            endif
c
c         output profiles every  so often
c
            if(mod(nt,ntsnap).eq.0)then
c
              write(14)time
              write(14)u,v,bprime,diff
c
            endif
c
          enddo
c
c         save endstate
c
          write(12)tmax,nz,zmax,u_0,S
          write(12)u,v,bprime,diff
          write(12)tstart
          write(12)tser,transport,l_depth
          write(12)N_over_f,C_d
          close(unit=12)
c
          time1=etime(utime,systime)
          write(9,20)utime/60.,systime/60.
20          format(' user and system time (min) used = ',2f7.2)
c
          close(unit=9)
c
          stop
c
1000          write(9,*)'execution stopped at t= ',tstart+float(nt)*dt
          write(9,*)'nsteps=',nsteps
c
          write(9,*)j,dfloat(j-1)*dz,u(j),v(j),bprime(j),diff(j),dfdz(j)
c
          do j=1,nz,10
             z=float(j-1)*dz
             write(9,9)z,u(j),v(j),bprime(j),diff(j),dfdz(j)
          enddo
c
          end
c*********************************************
c
```

```
c               CEOS : CEOR
c                University of Victoria
c                Victoria, BC V8W3P2
C
C*******************************************
c
c        module name: dave/models/mcr_exp/getpars.f
c
c        programmer's name: Dave Ramsden
c
c        date of writing: may 29 1992
c
c        date(s) of modification:
c
c        jul 17 1992:        add profiles of U,V,B,diff at different times
c        jul 28 1992:        add N/f and C_d
c        sep 11 1992:    add max diffusivity
c
c*********************************************************************
c        purpose: get run parameters for Richardson number dependence
c*********************************************************************
c
        subroutine getpars
c
        implicit none
c
        character*60 title
c
        real*8 s,tmax,zmax,u_0,dt_diag,prandtl,N_over_f,C_d,nu_max
c
        integer iostat,expnum,nz,nz_old,exp_old
c
        character*30 logfile,efile
c
        real*8 tstart,zmax_old,s_old,u_0_old
c
        common /params/S,tmax,zmax,u_0,tstart,dt_diag,prandtl
        1, N_over_f,C_d,nu_max
c
c*************************************************************
c
        namelist /startup/title     !title
        1,                s         !burger number
        1,                N_over_f  !N/f
        1,                C_d       !drag coefficient
        1,                prandtl   !Prandtl number
        1,                tmax      !time to stop integrations
```

```
      1,                dt_diag   !time inc. between diagnostics
      1,                zmax      !vertical extent
      1,                u_0       !alongslope velocity in the
c                                  far field
      1,                nu_max    !max value of nu in nondim units
      1,                exp_old   !the restart experiment number
c
      open(unit=8,file='../expnums.dat',iostat=iostat,status='old')
      if(iostat.ne.0)stop 'open error'
c
      read(8,1)expnum
      expnum=expnum+1
      rewind 8
      write(8,1)expnum
c
1      format(i5)
2      format(/,' Experiment number ',i5,/)
c
      close(unit=8)
c
      write(logfile,400)expnum
400      format('log',i4.4,'.dat')
      open(unit=9,file=logfile,iostat=iostat,status='new')
      if(iostat.ne.0)stop 'open logging error'
c
      write(efile,401)expnum
401      format('end',i4.4,'.dat')
      open(unit=12,file=efile,iostat=iostat,status='new'
      1,form='unformatted')
c
      if(iostat.ne.0)stop 'open end state file open error'
c
      open(unit=8,file='params.dat',iostat=iostat,status='old')
      if(iostat.ne.0)stop 'open error'
c
c      set max nu if not provided
c
      nu_max=.25
c
      read(8,nml=startup)
      close(unit=8)
c
      write(9,2)expnum
      write(9,nml=startup)
c
c      restart option
c
```

```
      if(exp_old.ne.0)then
        write(efile,401)exp_old
        open(unit=11,file=efile,iostat=iostat,status='old'
     1,form='unformatted')
c
        if(iostat.ne.0)stop 'open error on restart file'
c
        read(11)tstart,nz_old,zmax_old,u_0_old,s_old
c
      endif
c
c      update the parameter sweep history file
      open(unit=8,file='sweep.dat',iostat=iostat,status='old'
     1,access='append')
      if(iostat.ne.0)stop 'open error on sweep file'
c
      write(8,432)expnum,exp_old,S,prandtl,u_0,N_over_f,C_d
432      format(1x,2(i5,2x),5(e9.2,2x))
      close(unit=8)
c
c      open up a file for snapshots of u,v,b,diff
c
      write(efile,404)expnum
404      format('snap',i4.4,'.dat')
      open(unit=14,file=efile,iostat=iostat,status='new'
     1,form='unformatted')
c
      write(14)S,u_0,prandtl,zmax,N_over_f,C_d
c
      end
```

VITA

Surname: Ramsden Given Names: David

Place of Birth: London, England Date of Birth: April 4, 1949

Educational Instititions Attended:

Mcmaster University	1968 to 1972
University of Alberta	1972 to 1973

Degrees Awarded:

B. Eng.	1972

Publications:

Ramsden, D. and G. Holloway, 1992. Energy transfers across an internal wave-vortical mode spectrum, J. Geophys. Res., 97 (C3), 3659-3668.

Ramsden, D. and G. Holloway, 1991. Nonlinear energy transfers, Proc. 'Aha Hulikoa Hawaiian winter workshop, ed. P Muller and D. Henderson, 295-314.

Ramsden, D., and G. Holloway, 1987. Direct simulation and turbulence closure evaluation for large amplitude internal wave interactions in the vertical plane, Third Int'l Symp. Strat. Flows, Cal. Inst. Tech., Vol. 1.

Ramsden, D., 1987. Three Dimensional Stratified Turbulence, Final report on UP-I-191, Interact Computing Sevices private publication.

Tabata, S., B. Thomas and D. Ramsden, 1986. Annual and interannual variability of steric sea level along line P in the northeast Pacific ocean, J. Phys. Ocean., 16 (8), 1378-1398.

Holloway, G., S. C. Riser and D. Ramsden, 1986. Tracer anomaly evolution in the flow field of an isolated eddy, Dyn. Atmos. Oceans, 10, 165-184.

Thomson, R., S. Tabata and D. Ramsden, 1985. Comparison of sea level variability on the Caribbean and the Pacific coasts of the Panama canal. In time series of ocean measurements, Vol 2, IOC Tech. Ser. 30, Unesco.

Ramsden, D., D. Whitfield and G. Holloway, 1985. Spectral transform simulations of turbulent flows, with geophysical applications, Can. Tech. Rep. Hydrogr. Ocean Sci., No 57 54 pp.

Hill, G., D. Ramsden, W. A. Fisher, and S.C. Morris, 1982. The reduction of Spectra-I. VELMEAS, an interactive radial velocity program, Publ. Domin. Asrophys. Obs. Vol. XVI, No. 2.

PARTIAL COPYRIGHT LICENSE

Title of Thesis: Response of a Stably Stratified Oceanic Bottom Boundary Layer on a Slope to Time Dependent Forcing

Author [redacted]

DAVID RAMSDEN

April 27 1993